1-1-1997

The ZEUS Leading Proton Spectrometer and its Use in the Measurement of Elastic P^0 Photoproduction at HERA

M. Derrick
Argonne National Laboratory

D. Krakauer
Argonne National Laboratory

S. Magill
Argonne National Laboratory

D. Mikunas
Argonne National Laboratory

B. Musgrave
Argonne National Laboratory

DESY 96-183
August 1996

Study of Elastic ρ^0 Photoproduction at HERA using the ZEUS Leading Proton Spectrometer

ZEUS Collaboration

Abstract

The differential cross section $d\sigma/dt$ for elastic ρ^0 photoproduction, $\gamma p \to \rho^0 p$ ($\rho^0 \to \pi^+\pi^-$), has been measured in ep interactions at HERA. The squared four-momentum exchanged at the proton vertex, t, has been determined directly by measuring the momentum of the scattered proton using the ZEUS Leading Proton Spectrometer (LPS), a large scale system of silicon micro-strip detectors operating close to the HERA proton beam. The LPS allows the measurement of the momentum of high energy protons scattered at small angles with accuracies of 0.4% for the longitudinal momentum and 5 MeV for the transverse momentum. Photoproduction of ρ^0 mesons has been investigated in the interval $0.073 < |t| < 0.40$ GeV^2, for photon virtualities $Q^2 < 1$ GeV^2 and photon-proton centre-of-mass energies W between 50 and 100 GeV. In the measured range, the t distribution exhibits an exponential shape with a slope parameter $b = 9.8 \pm 0.8$ (stat.) ± 1.1 (syst.) GeV^{-2}. The use of the LPS eliminates the contamination from events with diffractive dissociation of the proton into low mass states.

The ZEUS Collaboration

M. Derrick, D. Krakauer, S. Magill, D. Mikunas, B. Musgrave, J.R. Okrasiński, J. Repond, R. Stanek, R.L. Talaga, H. Zhang
Argonne National Laboratory, Argonne, IL, USA [p]

M.C.K. Mattingly
Andrews University, Berrien Springs, MI, USA

F. Anselmo, P. Antonioli, G. Bari, M. Basile, L. Bellagamba, D. Boscherini, A. Bruni, G. Bruni, P. Bruni, G. Cara Romeo, G. Castellini[1], M. Chiarini, L. Cifarelli[2], F. Cindolo, A. Contin, M. Corradi, I. Gialas, P. Giusti, G. Iacobucci, G. Laurenti, G. Levi, A. Margotti, T. Massam, R. Nania, C. Nemoz, F. Palmonari, A. Pesci, A. Polini, G. Sartorelli, Y. Zamora Garcia[3], A. Zichichi
University and INFN Bologna, Bologna, Italy [f]

C. Amelung, A. Bornheim, J. Crittenden, R. Deffner, M. Eckert, L. Feld, A. Frey[4], M. Geerts[5], M. Grothe, H. Hartmann, K. Heinloth, L. Heinz, E. Hilger, H.-P. Jakob, U.F. Katz, S. Mengel[6], E. Paul, M. Pfeiffer, Ch. Rembser, D. Schramm[7], J. Stamm, R. Wedemeyer
Physikalisches Institut der Universität Bonn, Bonn, Germany [c]

S. Campbell-Robson, A. Cassidy, W.N. Cottingham, N. Dyce, B. Foster, S. George, M.E. Hayes, G.P. Heath, H.F. Heath, D. Piccioni, D.G. Roff, R.J. Tapper, R. Yoshida
H.H. Wills Physics Laboratory, University of Bristol, Bristol, U.K. [o]

M. Arneodo[8], R. Ayad, M. Capua, A. Garfagnini, L. Iannotti, M. Schioppa, G. Susinno
Calabria University, Physics Dept.and INFN, Cosenza, Italy [f]

A. Caldwell[9], N. Cartiglia, Z. Jing, W. Liu, J.A. Parsons, S. Ritz[10], F. Sciulli, P.B. Straub, L. Wai[11], S. Yang[12], Q. Zhu
Columbia University, Nevis Labs., Irvington on Hudson, N.Y., USA [q]

P. Borzemski, J. Chwastowski, A. Eskreys, Z. Jakubowski, M.B. Przybycień, M. Zachara, L. Zawiejski
Inst. of Nuclear Physics, Cracow, Poland [j]

L. Adamczyk, B. Bednarek, K. Jeleń, D. Kisielewska, T. Kowalski, M. Przybycień, E. Rulikowska-Zarębska, L. Suszycki, J. Zając
Faculty of Physics and Nuclear Techniques, Academy of Mining and Metallurgy, Cracow, Poland [j]

Z. Duliński, A. Kotański
Jagellonian Univ., Dept. of Physics, Cracow, Poland [k]

G. Abbiendi[13], L.A.T. Bauerdick, U. Behrens, H. Beier, J.K. Bienlein, G. Cases, O. Deppe, K. Desler, G. Drews, M. Flasiński[14], D.J. Gilkinson, C. Glasman, P. Göttlicher, J. Große-Knetter, T. Haas, W. Hain, D. Hasell, H. Heßling, Y. Iga, K.F. Johnson[15], P. Joos, M. Kasemann, R. Klanner, W. Koch, U. Kötz, H. Kowalski, J. Labs, A. Ladage, B. Löhr, M. Löwe, D. Lüke, J. Mainusch[16], O. Mańczak, J. Milewski, T. Monteiro[17], J.S.T. Ng, D. Notz, K. Ohrenberg, K. Piotrzkowski, M. Roco, M. Rohde, J. Roldán, U. Schneekloth, W. Schulz, F. Selonke, B. Surrow, E. Tassi, T. Voß, D. Westphal, G. Wolf, U. Wollmer, C. Youngman, W. Zeuner
Deutsches Elektronen-Synchrotron DESY, Hamburg, Germany

H.J. Grabosch, S.M. Mari[18], A. Meyer, S. Schlenstedt
DESY-IfH Zeuthen, Zeuthen, Germany

G. Barbagli, E. Gallo, P. Pelfer
University and INFN, Florence, Italy [f]

G. Anzivino, G. Maccarrone, S. De Pasquale, L. Votano
INFN, Laboratori Nazionali di Frascati, Frascati, Italy [f]

A. Bamberger, S. Eisenhardt, T. Trefzger[19], S. Wölfle
Fakultät für Physik der Universität Freiburg i.Br., Freiburg i.Br., Germany [c]

J.T. Bromley, N.H. Brook, P.J. Bussey, A.T. Doyle, D.H. Saxon, L.E. Sinclair, E. Strickland, M.L. Utley, R. Waugh, A.S. Wilson
Dept. of Physics and Astronomy, University of Glasgow, Glasgow, U.K. [o]

A. Dannemann[20], U. Holm, D. Horstmann, R. Sinkus[21], K. Wick
Hamburg University, I. Institute of Exp. Physics, Hamburg, Germany [c]

B.D. Burow[22], L. Hagge[16], E. Lohrmann, G. Poelz, W. Schott, F. Zetsche
Hamburg University, II. Institute of Exp. Physics, Hamburg, Germany [c]

T.C. Bacon, N. Brümmer, I. Butterworth, V.L. Harris, G. Howell, B.H.Y. Hung, L. Lamberti[23], K.R. Long, D.B. Miller, N. Pavel, A. Prinias[24], J.K. Sedgbeer, D. Sideris, A.F. Whitfield
Imperial College London, High Energy Nuclear Physics Group, London, U.K. [o]

U. Mallik, M.Z. Wang, S.M. Wang, J.T. Wu
University of Iowa, Physics and Astronomy Dept., Iowa City, USA [p]

P. Cloth, D. Filges
Forschungszentrum Jülich, Institut für Kernphysik, Jülich, Germany

S.H. An, G.H. Cho, B.J. Ko, S.B. Lee, S.W. Nam, H.S. Park, S.K. Park
Korea University, Seoul, Korea [h]

S. Kartik, H.-J. Kim, R.R. McNeil, W. Metcalf, V.K. Nadendla
Louisiana State University, Dept. of Physics and Astronomy, Baton Rouge, LA, USA [p]

F. Barreiro, J.P. Fernandez, R. Graciani, J.M. Hernández, L. Hervás, L. Labarga, M. Martinez, J. del Peso, J. Puga, J. Terron, J.F. de Trocóniz
Univer. Autónoma Madrid, Depto de Física Teóríca, Madrid, Spain [n]

F. Corriveau, D.S. Hanna, J. Hartmann, L.W. Hung, J.N. Lim, C.G. Matthews[25], W.N. Murray, A. Ochs, P.M. Patel, M. Riveline, D.G. Stairs, M. St-Laurent, R. Ullmann, G. Zacek[25]
McGill University, Dept. of Physics, Montréal, Québec, Canada [a], [b]

T. Tsurugai
Meiji Gakuin University, Faculty of General Education, Yokohama, Japan

V. Bashkirov, B.A. Dolgoshein, A. Stifutkin
Moscow Engineering Physics Institute, Mosocw, Russia [l]

G.L. Bashindzhagyan[26], P.F. Ermolov, L.K. Gladilin, Yu.A. Golubkov, V.D. Kobrin, I.A. Korzhavina, V.A. Kuzmin, O.Yu. Lukina, A.S. Proskuryakov, A.A. Savin, L.M. Shcheglova, A.N. Solomin, N.P. Zotov
Moscow State University, Institute of Nuclear Physics, Moscow, Russia [m]

M. Botje, F. Chlebana, J. Engelen, M. de Kamps, P. Kooijman, A. Kruse, A. van Sighem, H. Tiecke, W. Verkerke, J. Vossebeld, M. Vreeswijk, L. Wiggers, E. de Wolf, R. van Woudenberg[27]
NIKHEF and University of Amsterdam, Netherlands [i]

D. Acosta, B. Bylsma, L.S. Durkin, J. Gilmore, C.M. Ginsburg, C.L. Kim, C. Li, T.Y. Ling, P. Nylander, I.H. Park, T.A. Romanowski[28]
Ohio State University, Physics Department, Columbus, Ohio, USA [p]

D.S. Bailey, R.J. Cashmore[29], A.M. Cooper-Sarkar, R.C.E. Devenish, N. Harnew, M. Lancaster[30], L. Lindemann, J.D. McFall, C. Nath, V.A. Noyes[24], A. Quadt, J.R. Tickner, H. Uijterwaal, R. Walczak, D.S. Waters, F.F. Wilson, T. Yip
Department of Physics, University of Oxford, Oxford, U.K. [o]

A. Bertolin, R. Brugnera, R. Carlin, F. Dal Corso, M. De Giorgi, U. Dosselli, S. Limentani, M. Morandin, M. Posocco, L. Stanco, R. Stroili, C. Voci, F. Zuin
Dipartimento di Fisica dell' Universita and INFN, Padova, Italy [f]

J. Bulmahn, R.G. Feild[31], B.Y. Oh, J.J. Whitmore
Pennsylvania State University, Dept. of Physics, University Park, PA, USA [q]

G. D'Agostini, G. Marini, A. Nigro
Dipartimento di Fisica, Univ. 'La Sapienza' and INFN, Rome, Italy [f]

J.C. Hart, N.A. McCubbin, T.P. Shah
Rutherford Appleton Laboratory, Chilton, Didcot, Oxon, U.K. [o]

E. Barberis, T. Dubbs, C. Heusch, M. Van Hook, W. Lockman, J.T. Rahn, H.F.-W. Sadrozinski, A. Seiden, D.C. Williams
University of California, Santa Cruz, CA, USA [p]

J. Biltzinger, R.J. Seifert, O. Schwarzer, A.H. Walenta
Fachbereich Physik der Universität-Gesamthochschule Siegen, Germany [c]

H. Abramowicz, G. Briskin, S. Dagan[32], T. Doeker[32], A. Levy[26]
Raymond and Beverly Sackler Faculty of Exact Sciences, School of Physics, Tel-Aviv University, Tel-Aviv, Israel [e]

J.I. Fleck[33], M. Inuzuka, T. Ishii, M. Kuze, S. Mine, M. Nakao, I. Suzuki, K. Tokushuku, K. Umemori, S. Yamada, Y. Yamazaki
Institute for Nuclear Study, University of Tokyo, Tokyo, Japan [g]

M. Chiba, R. Hamatsu, T. Hirose, K. Homma, S. Kitamura[34], T. Matsushita, K. Yamauchi
Tokyo Metropolitan University, Dept. of Physics, Tokyo, Japan [g]

R. Cirio, M. Costa, M.I. Ferrero, S. Maselli, C. Peroni, R. Sacchi, A. Solano, A. Staiano
Universita di Torino, Dipartimento di Fisica Sperimentale and INFN, Torino, Italy [f]

M. Dardo
II Faculty of Sciences, Torino University and INFN - Alessandria, Italy [f]

D.C. Bailey, F. Benard, M. Brkic, C.-P. Fagerstroem, G.F. Hartner, K.K. Joo, G.M. Levman, J.F. Martin, R.S. Orr, S. Polenz, C.R. Sampson, D. Simmons, R.J. Teuscher
University of Toronto, Dept. of Physics, Toronto, Ont., Canada [a]

J.M. Butterworth, C.D. Catterall, T.W. Jones, P.B. Kaziewicz, J.B. Lane, R.L. Saunders, J. Shulman, M.R. Sutton
University College London, Physics and Astronomy Dept., London, U.K. [o]

B. Lu, L.W. Mo
Virginia Polytechnic Inst. and State University, Physics Dept., Blacksburg, VA, USA [q]

W. Bogusz, J. Ciborowski, J. Gajewski, G. Grzelak[35], M. Kasprzak, M. Krzyżanowski, K. Muchorowski[36], R.J. Nowak, J.M. Pawlak, T. Tymieniecka, A.K. Wróblewski, J.A. Zakrzewski, A.F. Żarnecki
Warsaw University, Institute of Experimental Physics, Warsaw, Poland [j]

M. Adamus
Institute for Nuclear Studies, Warsaw, Poland [j]

C. Coldewey, Y. Eisenberg[32], D. Hochman, U. Karshon[32], D. Revel[32], D. Zer-Zion
Weizmann Institute, Nuclear Physics Dept., Rehovot, Israel [d]

W.F. Badgett, J. Breitweg, D. Chapin, R. Cross, S. Dasu, C. Foudas, R.J. Loveless, S. Mattingly, D.D. Reeder, S. Silverstein, W.H. Smith, A. Vaiciulis, M. Wodarczyk
University of Wisconsin, Dept. of Physics, Madison, WI, USA [p]

S. Bhadra, M.L. Cardy[37], W.R. Frisken, M. Khakzad, W.B. Schmidke
York University, Dept. of Physics, North York, Ont., Canada [a]

[1] also at IROE Florence, Italy
[2] now at Univ. of Salerno and INFN Napoli, Italy
[3] supported by Worldlab, Lausanne, Switzerland
[4] now at Univ. of California, Santa Cruz
[5] now a self-employed consultant
[6] now at VDI-Technologiezentrum Düsseldorf
[7] now at Commasoft, Bonn
[8] also at University of Torino and Alexander von Humboldt Fellow
[9] Alexander von Humboldt Fellow
[10] Alfred P. Sloan Foundation Fellow
[11] now at University of Washington, Seattle
[12] now at California Institute of Technology, Los Angeles
[13] supported by an EC fellowship number ERBFMBICT 950172
[14] now at Inst. of Computer Science, Jagellonian Univ., Cracow
[15] visitor from Florida State University
[16] now at DESY Computer Center
[17] supported by European Community Program PRAXIS XXI
[18] present address: Dipartimento di Fisica, Univ. "La Sapienza", Rome
[19] now at ATLAS Collaboration, Univ. of Munich
[20] now at Star Division Entwicklungs- und Vertriebs-GmbH, Hamburg
[21] now at Philips Medizin Systeme, Hamburg
[22] also supported by NSERC, Canada
[23] supported by an EC fellowship
[24] PPARC Post-doctoral Fellow
[25] now at Park Medical Systems Inc., Lachine, Canada
[26] partially supported by DESY
[27] now at Philips Natlab, Eindhoven, NL
[28] now at Department of Energy, Washington
[29] also at University of Hamburg, Alexander von Humboldt Research Award
[30] now at Lawrence Berkeley Laboratory, Berkeley
[31] now at Yale University, New Haven, CT
[32] supported by a MINERVA Fellowship
[33] supported by the Japan Society for the Promotion of Science (JSPS)
[34] present address: Tokyo Metropolitan College of Allied Medical Sciences, Tokyo 116, Japan
[35] supported by the Polish State Committee for Scientific Research, grant No. 2P03B09308
[36] supported by the Polish State Committee for Scientific Research, grant No. 2P03B09208
[37] now at TECMAR Incorporated, Toronto

[a] supported by the Natural Sciences and Engineering Research Council of Canada (NSERC)

[b] supported by the FCAR of Québec, Canada

[c] supported by the German Federal Ministry for Education and Science, Research and Technology (BMBF), under contract numbers 057BN19P, 057FR19P, 057HH19P, 057HH29P, 057SI75I

[d] supported by the MINERVA Gesellschaft für Forschung GmbH, the Israel Academy of Science and the U.S.-Israel Binational Science Foundation

[e] supported by the German Israeli Foundation, and by the Israel Academy of Science

[f] supported by the Italian National Institute for Nuclear Physics (INFN)

[g] supported by the Japanese Ministry of Education, Science and Culture (the Monbusho) and its grants for Scientific Research

[h] supported by the Korean Ministry of Education and Korea Science and Engineering Foundation

[i] supported by the Netherlands Foundation for Research on Matter (FOM)

[j] supported by the Polish State Committee for Scientific Research, grants No. 115/E-343/SPUB/P03/109/95, 2P03B 244 08p02, p03, p04 and p05, and the Foundation for Polish-German Collaboration (proj. No. 506/92)

[k] supported by the Polish State Committee for Scientific Research (grant No. 2 P03B 083 08) and Foundation for Polish-German Collaboration

[l] partially supported by the German Federal Ministry for Education and Science, Research and Technology (BMBF)

[m] supported by the German Federal Ministry for Education and Science, Research and Technology (BMBF), and the Fund of Fundamental Research of Russian Ministry of Science and Education and by INTAS-Grant No. 93-63

[n] supported by the Spanish Ministry of Education and Science through funds provided by CICYT

[o] supported by the Particle Physics and Astronomy Research Council

[p] supported by the US Department of Energy

[q] supported by the US National Science Foundation

1 Introduction

The physics of diffractive scattering processes has emerged as one of the most interesting topics of study in the early running of HERA. Up to now, the cross section for events in which the virtual photon diffractively dissociates into a vector meson or a generic state X has been measured in the H1 and ZEUS experiments either by requiring a "large rapidity gap" between the proton beam direction and the most forward energy deposit recorded in the detector or by subtracting the non-diffractive background in a statistical way [1]-[7]. Here we present the first cross section measurement at HERA in which diffraction is tagged by the detection of a high energy scattered proton, thereby eliminating contamination by events with dissociation of the proton.

The measurement of the proton was performed using the ZEUS Leading Proton Spectrometer (LPS), which detects protons scattered at very small angles ($\lesssim$1 mrad). In this spectrometer, silicon micro-strip detectors are used in conjunction with the proton beam line elements to measure the momentum of the scattered proton. The detectors are positioned as close as the 10σ envelope of the circulating proton beam (typically a few mm) by using the "Roman pot" technique [8]. In the configuration used to collect the data presented here, the LPS consisted of a total of about 22,000 channels.

This paper concentrates on the exclusive process $\gamma p \to \rho^0 p$ in ep interactions at small photon virtualities ($Q^2 \approx 0$, the "photoproduction" region). This reaction is often called "elastic", in reference to the vector meson dominance model (VDM). Elastic photoproduction of ρ^0 mesons has been investigated in fixed target experiments at photon-proton centre-of-mass energies $W \lesssim 20$ GeV [9]-[11] as well as at HERA energies, $W \approx$ 100-200 GeV [2, 3]. The process has the characteristic features of soft diffractive interactions: the dependence of the cross section on W is weak, the dependence on t is approximately exponential, and the vector meson is observed to retain the helicity of the photon (s-channel helicity conservation). Here t is the squared four-momentum exchanged at the proton vertex. The data presented in this paper cover the kinematic range $50 < W < 100$ GeV, $Q^2 < 1$ GeV^2 and $0.073 < |t| < 0.40$ GeV^2. Elastic events were selected by requiring that the scattered proton carry more than 98% of the incoming proton beam energy. The scattered positron was not detected; however, Q^2 was estimated using transverse momentum balance.

2 Experimental set-up

2.1 HERA

The data discussed here were collected in 1994 at HERA which operated with 820 GeV protons and 27.5 GeV positrons (indicated in the following with the symbol e). The proton and positron beams each contained 153 colliding bunches, together with 17 additional unpaired proton and 15 unpaired positron bunches. These additional bunches were used for background studies. The time between bunch crossings was 96 ns. The typical instantaneous luminosity was 1.5×10^{30} cm^{-2}s^{-1} and the integrated luminosity for this study is 898 ± 14 nb^{-1}.

2.2 The ZEUS detector

A detailed description of the ZEUS detector can be found elsewhere [12]. A brief outline of the components in the central ZEUS detector [13] which are most relevant for this analysis is given below, followed by a description of the Leading Proton Spectrometer.

2.2.1 Central components and luminosity measurement

Charged particles are tracked by the inner tracking detectors which operate in a magnetic field of 1.43 T provided by a thin superconducting coil. Immediately surrounding the beam pipe is the vertex detector (VXD), a drift chamber which consists of 120 radial cells, each with 12 sense wires [14]. It is surrounded by the central tracking detector (CTD), which consists of 72 cylindrical drift chamber layers, organised into 9 superlayers covering the polar angle region $15^\circ < \theta < 164^\circ$[1] [15].

The high resolution uranium-scintillator calorimeter (CAL) [16] consists of three parts: the forward (FCAL), the rear (RCAL) and the barrel calorimeter (BCAL). Each part is subdivided transversely into towers and longitudinally into one electromagnetic section (EMC) and one (in RCAL) or two (in BCAL and FCAL) hadronic sections (HAC). A section of a tower is called a cell; each cell is viewed by two photomultiplier tubes. The CAL energy resolution, as measured under test beam conditions, is $\sigma_E/E = 0.18/\sqrt{E}$ for electrons and $\sigma_E/E = 0.35/\sqrt{E}$ for hadrons (E in GeV).

The Veto Wall, the C5 counter and the small angle rear tracking detector (SRTD) all consist of scintillation counters and are located at $Z = -730$ cm, $Z = -315$ cm and $Z = -150$ cm, respectively. Particles which are generated by proton beam-gas interactions upstream of the nominal ep interaction point hit the RCAL, the Veto Wall, the SRTD and C5 at different times than particles originating from the nominal ep interaction point. Proton beam-gas events are thus rejected by timing measurements in these detectors.

The luminosity is determined from the rate of the Bethe-Heitler process, $ep \to e\gamma p$, where the photon is measured with a calorimeter (LUMI) located in the HERA tunnel downstream of the interaction point in the direction of the outgoing positrons [17].

2.2.2 The Leading Proton Spectrometer

The Leading Proton Spectrometer [12] (LPS) detects charged particles scattered at small angles and carrying a substantial fraction, x_L, of the incoming proton momentum; these particles remain in the beam pipe and their trajectory is measured by a system of position sensitive silicon micro-strip detectors very close to the proton beam. The track deflection induced by the magnets in the proton beam line is used for the momentum analysis of the scattered proton.

The layout of the LPS is shown in Fig. 1; it consists of six detector stations, S1 to S6, placed along the beam line in the direction of the outgoing protons, at $Z = 23.8$ m, 40.3 m, 44.5 m, 63.0 m, 81.2 m and 90.0 m from the interaction point, respectively.

[1] The coordinate system used in this paper has the Z axis pointing in the proton beam direction, hereafter referred to as "forward", the X axis pointing horizontally towards the centre of HERA and the Y axis pointing upwards. The polar angle θ is defined with respect to the Z direction.

Each of the stations S1, S2 and S3 is equipped with an assembly of six planes of silicon micro-strip detectors parallel to each other and mounted on a mobile arm, which allows them to be positioned near the proton beam. Stations S4, S5 and S6 each consist of two halves, each half containing an assembly of six planes similar to those of S1, S2, S3, also mounted on mobile arms, as shown in Fig. 2. Each assembly has two planes with strips parallel to the direction of motion of the arm, two planes with strips at $+45^\circ$ and two at -45° with respect to it; this makes it possible to measure the particle trajectory in three different projections in each assembly. The dimensions of the detector planes vary from station to station but are approximately 4×6 cm^2. The pitch is 115 μm for the planes with vertical or horizontal strips and $115/\sqrt{2} = 81$ μm for the planes with $\pm 45^\circ$ strips. The distance along Z between neighbouring planes in an assembly is ≈ 7 mm. The detector planes are mounted in each assembly with a precision of about 30 μm.

The detector planes are inserted in the beam pipe by means of re-entrant "Roman pots" which allow the planes to operate at atmospheric pressure. A pot consists of a stainless steel cylinder with an open end away from the beam; the other end is closed. The silicon detector planes are inserted from the open end and are moved in until they are at about 0.5 mm from the closed end. The whole cylinder can be inserted transversely into the beam pipe. Figure 2 illustrates the principle of operation. The walls of the pots are 3 mm thick, except in front of and behind the detector planes, where they are 400 μm thick; the thickness of the pot bottom walls facing the beam is also 400 μm. The vacuum seal to the proton beam pipe is provided by steel bellows. The pots and the detector planes are positioned by remotely controlled motors and are retracted during the filling operations of the collider to increase the aperture of the vacuum chamber; this also minimises the radiation damage to the detectors and the front-end electronics. In stations S1, S2, S3 the detector planes are inserted into the beam pipe horizontally from the outside of the HERA ring towards the centre. In stations S4, S5, S6, the detector planes in the two halves of each station independently approach the beam from above and from below. In the operating position the upper and lower halves partially overlap (cf. Fig. 2). The offset along the beam direction between the centres of the upper and lower pots is ≈ 10 cm. Stations S5 and S6 were used in an earlier experiment at CERN and were adapted to the HERA beam line [18].

Each detector plane has an elliptical cutout which follows the profile of the 10σ envelope of the beam, where σ is the standard deviation of the spatial distribution of the beam in the transverse plane. Since the 10σ profile differs from station to station, the shape of the cutout varies from station to station; in data taking conditions the distance of each detector from the beam centre is also different and ranges from 3 to 20 mm. Small variations of the detector positions from fill to fill are necessary during operation in order to follow the changes of the beam position and adapt to the background conditions.

The detector planes are read out by two types of VLSI chips mounted on the detector support: a bipolar amplifier-comparator [19] followed by a radiation hard CMOS digital pipeline [20], which operates with a clock frequency of 10.4 MHz, synchronous with the HERA bunch crossing. Each chip has 64 channels reading out 64 adjacent strips. The chips are radiation hard up to doses of several Mrad.

A simplified diagram of the spectrometer optics is shown in Fig. 3, in which the beam line elements have been combined to show the main optical functions. Together with the HERA proton beam magnets, the six LPS stations form two spectrometers:

1. Stations S1, S2, S3 use the combined horizontal bending power of a septum magnet and three magnetic septum half-quadrupoles. S1, S2, S3 were not operational in 1994 and are not discussed further here.

2. Stations S4, S5, S6 exploit in addition the vertical bending provided by three main dipole magnets (BU). These stations were used for the present measurement.

The insertion of the detectors into the operating positions typically begins as soon as the beams are brought into collision. Among the conditions required prior to beginning the insertion are the following: (i) proton beam position as measured with the HERA beam position monitor next to S4 within 1 mm of the nominal position; (ii) background levels as measured in counters downstream of the main proton beam collimators, in the C5 counter and in the trigger counters of the Forward Neutron Calorimeter [21] (located downstream of S6 at $Z \approx 109$ m) stable and below given thresholds. About fifty minutes were necessary in 1994 to insert the detector planes. This and the fact that the beam conditions did not always allow safe insertion of the detectors results in the reduced value of the integrated luminosity available for this analysis with respect to other analyses of the ZEUS 1994 data.

The strip occupancy during data taking, i.e. the average number of strips firing per trigger divided by the total number of strips, depended on the beam conditions but was typically less than 0.1%, with small contributions from noise and synchrotron radiation.

The fraction of noisy and malfunctioning channels in 1994 was less than 2%; they were due to bad detector strips and dead or noisy front-end channels. The efficiency of the detector planes, after excluding these channels, was better than 99.8%.

The LPS accepts scattered protons carrying a fraction of the beam momentum, x_L, in the range $x_L \gtrsim 0.4$ and with $0 \lesssim p_T \lesssim 1$ GeV, where p_T is the transverse momentum of the proton with respect to the incoming beam direction. With the configuration installed in 1994 (S4, S5, S6), the resolution in x_L is better than 0.4% at 820 GeV and the p_T resolution is about 5 MeV. The latter is less than the intrinsic transverse momentum spread in the proton beam at the interaction point (with rms of about 40 MeV horizontally and about 90 MeV vertically) due to the beam divergence of ≈ 50 μrad in the horizontal and ≈ 110 μrad in the vertical plane. The LPS resolution is further discussed in section 3.1.2.

2.2.3 Reconstruction of an LPS track

Tracks are reconstructed in stages, proceeding from individual hits to full tracks [22]. Noisy and malfunctioning channels are masked out and clusters of adjacent hit strips are searched for in each detector plane. Most clusters are one strip wide only (typically $\approx 25\%$ of the clusters have more than 1 strip). Track segments are then found independently in each detector assembly of six planes. As a first step, matching clusters in the two planes with the same strip orientation are combined. Candidate local track segments are then found by combining pairs of clusters belonging to different projections; when a pair of such clusters intersects within the region covered by the sensitive area of the detectors, a corresponding cluster in the remaining projection is searched for. In order to reduce the number of candidates, local track segments that traverse the overlap region of the detectors in the upper and the lower halves of the station are treated as one candidate. Finally, all hits belonging to a candidate (up to twelve for tracks

crossing the two halves, up to six otherwise) are used in a fit to find the transverse coordinates of the track at the value of Z corresponding to the centre of the station. The spatial resolution on these coordinates is about 30 μm. Figure 4 shows the position of the reconstructed coordinates in the stations S4, S5 and S6 for a typical run. The regions with a high density of reconstructed hits in the overlap zone between the upper and the lower detectors correspond to tracks with x_L close to unity. Lower x_L tracks are deflected upwards and focussed horizontally onto a vertical line. For x_L close to unity, this focus line is downstream of S6; it approaches S6 as x_L decreases and reaches S6 for $x_L \approx 0.7$. This explains the fact that for low x_L tracks, the impact points in S5 and S6 tend to lie in a region which becomes narrower as the vertical coordinate increases.

We distinguish two classes of events: those which are detected in all three of the stations and those which are detected in only two stations. In the latter, the interaction vertex position is required as a third point to measure the momentum. Tracks detected in three stations can be extrapolated backwards to $Z = 0$ to also measure the transverse position of the interaction vertex. In both cases, coordinates reconstructed in pairs of different stations are first combined into track candidates and the track momentum is determined using the average ep interaction vertex with coordinates (X_0, Y_0), found on a run-by-run basis with the sample of three-station tracks. Linear matrix equations relate the horizontal and vertical coordinates of the positions (h_k, v_k) and slopes ($h'_k = dh_k/dl$, $v'_k = dv_k/dl$) of the track at each station to the position (X_0, Y_0) and slope (X'_0, Y'_0) of the track at the interaction point. The coordinate along the beam trajectory is l. The positions (h_k, v_k) and slopes (h'_k, v'_k) are relative to the nominal beam position and direction at that value of l. The nominal beam crosses the interaction point $(Z = 0)$ at $X = Y = 0$. For the horizontal direction one has:

$$\begin{pmatrix} h_k \\ h'_k \end{pmatrix} = \begin{pmatrix} m_0 & m_1 \\ m_2 & m_3 \end{pmatrix} \begin{pmatrix} X_0 \\ X'_0 \end{pmatrix} + \begin{pmatrix} b_0 \\ b_1 \end{pmatrix}. \tag{1}$$

An independent equation of the same form can be written for the vertical direction. The matrix elements m_i are known functions of x_L which describe the beam optics including the effects of quadrupoles and drift lengths. The quantities (b_0, b_1), also functions of x_L, describe the deflection induced by the dipoles and by the quadrupoles in which the beam is off axis; since the beam is taken as reference, they vanish as $x_L \to 1$.

Equation (1) and the corresponding one for the vertical direction can be written for a pair of stations (a, b); upon eliminating the unknowns X'_0 and Y'_0, one finds

$$h_b = M_h^{ab}(x_L) h_a + C_h^{ab}(x_L, X_0), \tag{2}$$
$$v_b = M_v^{ab}(x_L) v_a + C_v^{ab}(x_L, Y_0), \tag{3}$$

where M^{ab} and C^{ab} are functions of the matrix elements m_i and b_i. These two equations are independent, apart from the common dependence on x_L, and can be used to obtain two independent estimates of x_L. If the values obtained are compatible, the pair of coordinates is retained as a candidate two-station track.

As a final step of the pattern recognition, three-station track candidates are searched for using pairs of two-station candidates, e.g. one in S4, S5 and another in S5, S6. If a pair uses

the same hits in the station common to the two tracks, if the projections of the two tracks on the horizontal (non-bending) plane coincide and if the momenta assigned to each track are compatible, then the two candidates are merged in a three-station track candidate. Two-station and three-station candidates are then passed to a conventional track-fitting stage.

A track χ^2 is defined as

$$\chi^2 = \left[\sum_i \frac{(s_i - S_i(\psi))^2}{\sigma_i^2}\right] + \frac{(X_V - X_0)^2}{\sigma_{X_V}^2} + \frac{(Y_V - Y_0)^2}{\sigma_{Y_V}^2}, \tag{4}$$

where the sum runs over all clusters in all planes assigned to a track. Here s_i is the cluster position, σ_i the uncertainty associated to it (which includes the effects of multiple scattering and the contribution of the cluster width; typical values range from 50 to 100 μm), (X_V, Y_V) the interaction vertex coordinates in the X, Y plane, σ_{X_V} and σ_{Y_V} the nominal widths of the vertex distribution; S_i, a function of the five track parameters $\psi = (X_V, Y_V, X'_V, Y'_V, x_L)$, is the predicted cluster position calculated from equation (1) and the corresponding one in the vertical direction; the quantities X'_V, Y'_V indicate the track slopes at the interaction vertex. The last two terms in eq. (4) constrain the track to the interaction vertex. This χ^2 is minimised with respect to the five track parameters, and the best track parameters, together with the error matrix, are determined. In the present analysis, for x_L close to unity, the average value of χ^2/ndf is ≈ 1, where ndf is on average 7.3 for two-station tracks and 17.3 for three-station tracks. Three-station tracks are 60% of the total.

2.2.4 Alignment of the LPS

The alignment of the LPS relies on survey information for locating the detector planes in l and on high-energy proton tracks for locating them in h and v. The individual detector planes are first aligned within one station, then the relative alignment of the stations is determined, and finally the three stations S4, S5, S6 are aligned relative to the ZEUS detector. Typical accuracies in h and v are better than 20 μm. The actual path of the proton beam is also determined. These steps are described below.

Tracks traversing the region in which the active areas of the detector planes in the upper and lower halves of a station overlap are used to align the detector planes within each half as well as to determine the position of the upper with respect to the lower half. With this procedure each plane is aligned independently; rotations of the detectors around the l axis are also determined.

The relative alignment between the S4, S5, S6 stations in h is then found by exploiting the fact that tracks are straight lines in this projection.

The only magnetic elements between S4 and S6 are the dipoles between S4 and S5 which deflect particles vertically. A sample of tracks with known deflection (i.e. known momentum) is thus necessary to align the stations relative to each other in v. This can be obtained independently of the LPS using the ZEUS calorimeter:

$$x_L^{CAL} = 1 - \sum_i (E_i + p_{Zi})/(2E_p), \tag{5}$$

where the sum runs over all calorimeter cells, E is the energy measured in each cell and $p_Z = E\cos\theta$, with θ the polar angle of each cell. The symbol E_p denotes the incoming proton energy. Equation (5) follows from energy and momentum conservation: $\sum(E+p_Z)_{IN} = \sum(E+p_Z)_{OUT}$, where the sums run over the initial and final state particles, respectively, and $\sum(E+p_Z)_{IN} = 2E_p$. Events are selected with $x_L^{CAL} > 0.99$; these events have a clear peak in the x_L spectrum as measured by the LPS, with very little background underneath. The relative positions of the stations are adjusted so that the peak appears at x_L of unity. For the 1994 data, about 20,000 events were used. The vertical alignment is finally checked by using events with elastic photoproduction of ρ^0 mesons – those discussed in the present paper – exploiting the fact that these events have scattered protons with x_L very close to unity: x_L can be written, for elastic ρ^0 photoproduction, as $x_L = 1 - (Q^2 + M_\rho^2 + |t|)/W^2$, where M_ρ is the ρ^0 meson mass; for the sample used, the value of x_L differs from unity by at most 0.2%.

In order to align S4, S5 and S6 with respect to the proton beam line, tracks traversing all three stations are extrapolated to $Z = 0$, taking into account the fields of all traversed magnetic elements (mostly quadrupoles, as shown in Fig. 1). The detectors are aligned with respect to the quadrupole axes by requiring that, independent of x_L, the average position of the extrapolated vertex be the same as that measured by the central tracking detectors. At this point the detectors are aligned relative to the proton beam line and to the HERA quadrupole axes, and hence to the other components of ZEUS. About 40,000 three-station tracks were used for this procedure.

Finally, the average angle of the proton beam with respect to the nominal beam direction is determined by using events of elastic photoproduction of ρ^0 mesons. For such events the transverse components of the scattered proton momentum balance on average those of the ρ^0 meson. The mean value of the sum of p_X^{LPS} and p_X^{CTD}, and similarly for p_Y, is set to zero by adding a constant offset to the fitted angle of the LPS tracks at the interaction vertex for all events. Here p_X^{LPS} and p_X^{CTD} indicate the X component of the proton momentum as measured by the LPS and of the ρ^0 momentum as measured by the CTD, respectively. This procedure defines the direction of the Z axis. Typical values of the beam offset are -15 μrad and -100 μrad in the horizontal and vertical directions, respectively, with respect to the nominal beam direction. The 1994 running period was split into three parts during which the beam tilt was relatively constant and the offset was determined for each part. Fig. 5 shows, separately for the X and Y projections, the sum of the proton and the ρ^0 transverse momenta after this correction, which is determined by requiring that both histograms be centred on zero. The width of the distributions is dominated by the intrinsic spread of the transverse momentum in the beam. The other (minor) contributions are the LPS and CTD resolutions and the fact that the transverse momentum of the scattered positron is not identically zero since Q^2 is not zero. Note that the effect of non-zero Q^2 is just to widen the distributions of Fig. 5, not to shift them, since the X and Y components of the scattered positron momentum are centred on zero. In addition events with $Q^2 \gtrsim 0.01$ GeV^2 contribute to the non-Gaussian tails. The x_L scale is not affected by this tilt correction. The sensitivity of the determination of t to the value of the tilt is weak, as discussed in section 4. The effect of this correction is negligible for all quantities measured in the central ZEUS apparatus.

As mentioned earlier, the detectors are in the retracted position between HERA runs; the positions of the pots (and hence of the detector planes) vary from one proton fill to the next by up to a few millimeters in Y (rarely in X) depending on the beam position and on the background conditions. Coordinate reconstruction can thus not be more accurate than the

reproducibility of the detector positioning system folded with the alignment accuracy. This is monitored by the run-to-run dependence of the difference between the coordinates of the track impact point as measured by the detector planes in the upper and lower halves of a station for tracks in the overlap region. Note that this can be done since the alignment procedure described above is carried out using data from the whole running period, i.e. not on a run-by-run basis. The rms value of this difference is ≈ 25 μm and is consistent with the specifications of the mechanics and commensurate with the detector resolution.

3 Analysis

3.1 Event selection

3.1.1 Trigger

ZEUS uses a three-level trigger system [12, 13]. For the present data, the trigger selected events with photoproduction of a vector meson decaying into two charged particles with no requirement that either the scattered positron or the scattered proton be detected.

The first-level trigger required an energy deposit of at least 464 MeV in the electromagnetic section of RCAL (excluding the towers immediately around the beam pipe) and at least one track candidate in the CTD. Events with an energy deposit larger than 1250 MeV in the FCAL towers surrounding the beam pipe were rejected in order to suppress proton beam-gas events along with a large fraction of other photoproduction events. No requirements were made on the LPS information.

At the second-level trigger, the background was reduced by using the measured times of the energy deposits and the summed energies from the calorimeter.

The full event information was available at the third-level trigger; however, only a simplified reconstruction procedure was used. Tighter timing cuts as well as algorithms to remove cosmic muons were applied. One reconstructed vertex was demanded, with a Z coordinate within ± 66 cm of the nominal interaction point. Furthermore, the events were required to satisfy at least one of the following conditions:

1. fewer than four reconstructed tracks and at least one pair with invariant mass less than 1.5 GeV (assuming they are pions);

2. fewer than six reconstructed tracks and no pair with invariant mass larger than 5 GeV (again assuming pions).

Both sets of third-level triggers were prescaled by a factor six. Approximately 3×10^5 events were selected in this way, from an integrated luminosity of 898 ± 14 nb^{-1} (the luminosity corresponding to no prescale).

3.1.2 Offline requirements

After performing the full reconstruction of the events, the following offline requirements were imposed to select elastic $\rho^0 \to \pi^+\pi^-$ candidates with a high momentum scattered proton:

- Exactly two tracks in the CTD from particles of opposite charge, both associated with the reconstructed vertex.
- The Z coordinate of the vertex within ± 30 cm and the radial distance within 1.5 cm of the nominal interaction point.
- In BCAL and RCAL, not more than 200 MeV in any EMC (HAC) calorimeter cell which is more than 30 cm (50 cm) away from the extrapolated impact position of either of the two tracks. This cut rejects events with additional particles, along with events with the scattered positron in RCAL.
- One track in the LPS with $0.98 < x_L < 1.02$. This corresponds to a $\pm 5\sigma$ window around $x_L = 1$, for an x_L resolution of 0.4%. As stated in section 2.2.4, elastic photoproduction of ρ^0 mesons peaks at values of x_L which differ from unity by less than 2×10^{-3}. This requirement is used to tag elastic events.
- Protons whose reconstructed trajectories come closer than 0.5 mm to the wall of the beam pipe, at any point between the vertex and the last station hit, were rejected. This eliminates events where the proton could have hit the beam pipe wall and showered. In addition, it removes any sensitivity of the acceptance to possible misalignments of the HERA beam pipe elements.
- The value of the χ^2/ndf of the fit to the proton track (cf. section 2.2.3) less than 6.

The pion mass was assigned to each CTD track and the analysis was restricted to events reconstructed in the kinematic region defined by:

$$\begin{aligned} 0.55 < \quad & M_{\pi\pi} & < 1.2 \text{ GeV}, \\ 0.27 < \quad & p_T & < 0.63 \text{ GeV}, \\ 50 < \quad & W & < 100 \text{ GeV}, \\ & Q^2 & < 1 \text{ GeV}^2. \end{aligned} \tag{6}$$

The restricted range in the two-pion invariant mass $M_{\pi\pi}$ reduces the contamination from reactions involving other vector mesons, in particular from elastic ϕ and ω production. The limits on p_T, which is measured with the LPS, remove regions in which the acceptance of the LPS changes rapidly (cf. section 3.2).

The photon-proton centre-of-mass energy W and the mass $M_{\pi\pi}$ were determined from the momenta of the two pions [2]. Energy and momentum conservation relate the photon energy, E_γ, to the two-pion system energy $E_{\pi\pi}$ and longitudinal momentum $p_{Z\pi\pi}$ by $2E_\gamma \approx (E_{\pi\pi} - p_{Z\pi\pi})$, under the assumption that the positron emits the virtual photon with zero transverse momentum. Therefore $W^2 \approx 4E_\gamma E_p \approx 2(E_{\pi\pi} - p_{Z\pi\pi})E_p$. From the Monte Carlo study discussed

in the next section, the resolution on W has been found to be about 2 GeV; that on $M_{\pi\pi}$ is about 30 MeV.

The combination of the trigger requirements and the offline cuts, excluding that on Q^2, limits Q^2 to be less than ≈ 4 GeV^2. However, unlike previous ZEUS analyses of untagged photoproduction events, for the present data Q^2 was determined event by event. By exploiting the transverse momentum balance of the scattered positron, the $\pi^+\pi^-$ pair and the scattered proton, one obtains p_T^e, the transverse momentum of the scattered positron. The variable Q^2 was then calculated from $Q^2 = (p_T^e)^2/(1-y)$, where y is the fraction of the positron energy transferred by the photon to the hadronic final state, in the proton rest frame; it was evaluated as $y \approx W^2/s$, where $\sqrt{s}$ is the ep centre-of-mass energy. Figure 6 shows a scatter plot of the reconstructed and the generated value of Q^2 for the sample of Monte Carlo events used to evaluate the acceptance (cf. section 3.2); the line shows the expected average relationship between these two quantities assuming a beam transverse momentum distribution with $\sigma_{p_X} = 40$ MeV and $\sigma_{p_Y} = 90$ MeV. At small values of Q^2, the resolution on Q^2 is dominated by the beam transverse momentum spread; it is about 100% at 3×10^{-2} GeV^2, 40% at 0.1 GeV^2 and 20% at 1 GeV^2.

The final sample contains 1653 events. Figure 7 shows the $M_{\pi\pi}$, W, p_X, p_Y, p_T and x_L distributions after the offline selections; the variables p_X and p_Y denote the transverse components of the outgoing proton momentum with respect to the incoming beam axis and $p_T^2 = p_X^2 + p_Y^2$. The invariant mass plot is dominated by the ρ^0 peak. The shape of the p_X spectrum, with two well separated peaks, is a consequence of the fact, discussed earlier, that events with x_L close to unity only populate a narrow region of the detectors at $v \approx 0$. As discussed earlier, elastic ρ^0 photoproduction peaks at $x_L = 1$ to within $< 2\times10^{-3}$; the width of the x_L distribution in Fig. 7f shows that the resolution of the LPS in x_L is $\approx 0.4\%$. For the same events, Fig. 8 shows the scatter plot of the reconstructed X and Y components of the proton momentum. For the present measurement, only the p_T region between the dashed vertical lines in Fig. 7e was used. The variable $t = (p-p')^2$, where p and p' are the incoming and the scattered proton four-momenta, respectively, can be evaluated as follows:

$$t = (p-p')^2 \approx -\frac{p_T^2}{x_L}\left[1 + (M_p^2/p_T^2)(x_L-1)^2\right], \tag{7}$$

where M_p is the proton mass and terms of order $(M_p^2/\vec{p'}^2)^2$ or higher are neglected. For the present events, which have $x_L \approx 1$, the approximation $t \approx -p_T^2/x_L \approx -p_T^2$ was used.

Finally, Fig. 9 shows the distribution of the reconstructed values of Q^2. As discussed above, at small values of Q^2 the intrinsic spread of the beam transverse momentum dominates. The requirement that Q^2 be less than 1 GeV^2 removes 7 events. The median Q^2 of the data, estimated with the Monte Carlo study discussed in the next section, is approximately 10^{-4} GeV^2.

3.2 Monte Carlo generators and acceptance calculation

The reaction $ep \to e\rho^0 p$ was modelled using the DIPSI [23] generator, which was shown to reproduce the ZEUS ρ^0 photoproduction data [2]. The effective W dependence of the γp cross section for the events generated was of the type $\sigma \propto W^{0.2}$. The t distribution was approximately exponential with a slope parameter of 9.5 GeV^{-2}. The two-pion invariant mass, $M_{\pi\pi}$, was

generated so as to reproduce, after reconstruction, the measured distribution. The angular distribution of the decay pions was assumed to be that expected on the basis of s-channel helicity conservation [24].

The simulated events were passed through the same reconstruction and analysis programs as the data. In Figures 7 and 9 the distributions of the reconstructed data (not corrected for acceptance) over $M_{\pi\pi}$, W, p_X, p_Y, p_T, x_L and Q^2 are compared with those obtained for the reconstructed Monte Carlo events. The Monte Carlo is in reasonable agreement with the data. Figure 10a shows the overall acceptance as a function of t, obtained using DIPSI. The acceptance includes the effects of the geometric acceptance of the apparatus, its efficiency and resolution and the trigger and reconstruction efficiencies. Since the detector planes cannot be positioned in the beam, the acceptance vanishes at small values of t. Conversely, in the p_X, p_Y region covered by the detectors, the acceptance of the LPS is large, as shown in Fig. 10b, which shows the geometric acceptance of the LPS alone, irrespective of the acceptance of the rest of the ZEUS apparatus. The region of LPS geometric acceptance larger than 95% for both $p_X > 0$ and $p_X < 0$ maps into that of $0.25 \lesssim p_T \lesssim 0.65$ GeV; as discussed in section 3.1.2, events outside this region are not used in the present analysis. For events with elastic ρ^0 photoproduction, the geometric acceptance of the LPS, averaged over azimuth, is approximately 6%.

As discussed in the next section, in order to estimate the contamination from the reaction $ep \to e\rho^0 X_N$, where X_N is a hadronic state of mass M_N resulting from the diffractive dissociation of the proton, the PYTHIA generator [25] was used. A cross section of the form $d^2\sigma/dtdM_N^2 \propto e^{-b|t|}/M_N^2$, with $b = 6$ GeV^{-2}, was assumed; the value of M_N ranged between $M_p + M_\pi$ (where M_p is the proton and M_π the pion mass) and a maximum fixed by the condition $M_N^2/W^2 \leq 0.1$ [26]. The ρ^0 decay angular distributions were assumed to be the same as those of the elastic events.

3.3 Backgrounds

After applying the selection criteria described in section 3.1, the data contain small contributions from various background processes to the reaction $ep \to e\pi^+\pi^- p$:

- Beam-halo tracks observed in the LPS may overlap with events in which a ρ^0 is seen by the ZEUS central apparatus. The term beam-halo refers to protons with energy close to that of the beam originating from interactions of beam protons with the residual gas in the pipe or with the beam collimators. Such tracks are completely uncorrelated with the activity in the central ZEUS apparatus; therefore, any sample of events selected without using the LPS information contains the same fraction, ϵ_{halo}, of random overlaps from halo tracks within the LPS acceptance. This fraction was found to be $\epsilon_{halo} = 0.25 \pm 0.03\%$ by analysing events of the type $ep \to eX$ at $Q^2 > 4$ GeV^2 in which the virtual photon diffractively dissociates into the state X. For these events one can measure X and the scattered positron in the calorimeter; in addition a proton track is looked for in the LPS. If one is found, the event is fully contained and its kinematics is thus overconstrained: most beam-halo events appear to violate energy-momentum conservation and can therefore be identified.

  The contamination of the present sample (after the requirement of a good LPS track) can be obtained as $(\epsilon_{halo} N_{noLPS})/N_{LPS} = 5.0\% \pm 0.6\%$ (stat.), where N_{noLPS} indicates

the number of events found by applying all cuts except for the requirement that a track be detected in the LPS, and $N_{LPS} = 1653$ is the number of events after all cuts. These events were not removed from the present sample, but their effect on the measurement of the t slope is small, as discussed in section 4.

- In the reaction $ep \to e\rho^0 X_N$, the proton diffractively dissociates into a hadronic state X_N which may escape detection by the central detector. The debris of X_N may contain a proton within the LPS acceptance and with $0.98 < x_L < 1.02$: such events are indistinguishable from elastic ρ^0 production.

  In order to evaluate the contamination from such events, the cut on x_L was removed; Fig. 11 shows the x_L spectrum thus obtained, not corrected for acceptance. The sum of the reconstructed x_L distributions from DIPSI and PYTHIA was fitted to this spectrum with the normalisations of the simulated distributions as free parameters of the fit. The fit gives an acceptable description of the data, as shown in Fig. 11. The resulting contamination of proton-dissociative events for $x_L > 0.98$ is $0.21\% \pm 0.15\%$ (stat.), a major improvement with respect to $11\% \pm 1\%$ (stat.) $\pm 6\%$ (syst.) in the earlier ZEUS result [2] which did not use the LPS.

- The contaminations from elastic production of ω and ϕ mesons were estimated in [2] to be $(1.3 \pm 0.2)\%$ and $(0.3 \pm 0.1)\%$, respectively.

- Contamination from positron beam-gas and proton beam-gas events was studied by using the unpaired bunches event samples to which all the cuts described above were applied. No event passed the cuts, indicating a negligible contamination.

4 Results

The differential cross section $d\sigma/dM_{\pi\pi}$ for the process $\gamma p \to \pi^+\pi^- p$ was evaluated in the kinematic range $0.55 < M_{\pi\pi} < 1.2$ GeV, $50 < W < 100$ GeV, $Q^2 < 1$ GeV^2 and $0.073 < |t| < 0.40$ GeV^2. In each bin the cross section was obtained as

$$\frac{N_{\pi^+\pi^-}}{aL\Phi} c_{halo}, \tag{8}$$

where $N_{\pi^+\pi^-}$ is the number of observed events in the bin, L is the integrated luminosity, a is the overall acceptance in the bin, and $\Phi = 0.0574$ is the photon flux factor, i.e. the integral of equation (5) in ref. [2] over the measured W and Q^2 ranges of this measurement. The factor $c_{halo} = 0.950 \pm 0.006$ (stat.) corrects for the beam-halo contamination discussed in section 3.3.

The effects of positron initial and final state radiation and that of vacuum polarisation loops were neglected; the effects on the integrated cross section were estimated to be smaller than 4% [28]. The effects on the shape of the $M_{\pi\pi}$ and t distributions are expected to be negligible. The small residual contaminations from proton dissociative ρ^0 production and elastic ω and ϕ production, discussed in the previous section, were not corrected for.

Figure 12 shows the differential cross section $d\sigma/dM_{\pi\pi}$ in the interval $0.55 < M_{\pi\pi} < 1.2$ GeV, $0.073 < |t| < 0.40$ GeV^2 for $\langle W \rangle = 73$ GeV. The mass spectrum is skewed, as previously

observed both at low energy and at HERA. This can be understood in terms of resonant and non-resonant $\pi^+\pi^-$ production [29], and their interference [30]. The spectrum was fitted using expression (11) of ref. [2]. The results for the total, resonant and interference terms, as obtained in the fit, are indicated in the figure. The fraction of the resonant to the total contribution in the measured range was found to be $c_{res} = 0.91 \pm 0.04$ (syst.). The uncertainty was evaluated by repeating the fit with the various functional forms discussed in [2]. In [2] the contribution of the resonant term was found to vary from 86% for $|t| = 0.01$ GeV^2 to 95% for $|t| = 0.5$ GeV^2. No t dependence of c_{res} was assumed here, except in the evaluation of the systematic uncertainty (see below).

The differential cross section $d\sigma/dt$ for the reaction $\gamma p \to \rho^0 p$ was obtained similarly to $d\sigma/dM_{\pi\pi}$, but in addition the correction factor c_{res}, just discussed, was applied. Figure 13 shows the result in the interval $0.073 < |t| < 0.40$ GeV^2, $0.55 < M_{\pi\pi} < 1.2$ GeV for $\langle W \rangle = 73$ GeV. The data were fitted with the function

$$\frac{d\sigma}{dt} = A \cdot e^{-b|t|}; \tag{9}$$

the result of the fit is shown as a straight line on Fig. 13. The fitted value of the slope parameter b is

$$b = 9.8 \pm 0.8 \text{ (stat.)} \pm 1.1 \text{ (syst.) GeV}^{-2}. \tag{10}$$

The result is consistent with $b = 9.9 \pm 1.2$ (stat.) ± 1.4 (syst.) GeV^{-2} obtained in [2] for the range $60 < W < 80$ GeV, $Q^2 < 4$ GeV^2 and $|t| < 0.5$ GeV^2 using a fit of the type $A \exp(-b|t| + ct^2)$. For both the present data and those of ref. [2], $\langle W \rangle \approx 70$ GeV.

The measured differential cross section was integrated over the range $0.073 < |t| < 0.40$ GeV^{-2}, yielding $\sigma = 5.8 \pm 0.3$ (stat.) ± 0.7 (syst.) μb, again at $\langle W \rangle = 73$ GeV and for $0.55 < M_{\pi\pi} < 1.2$ GeV. The result can be extrapolated to the mass range $2M_\pi < M_{\pi\pi} < M_\rho + 5\Gamma_0$, as in [2], using the fit to the mass spectrum described earlier (here Γ_0 is the ρ^0 width); this yields $\sigma = 6.3 \pm 0.3$ (stat.) ± 0.8 (syst.) μb, where no uncertainty was assigned to the extrapolation. If our previous result [2] is integrated in the t range covered by the present data, using the published results of the fit with the function $A \exp(-b|t| + ct^2)$ (table 5 of ref. [2], left column), one finds $\sigma = 6.7 \pm 1.1$ (syst.) μb, in good agreement with the present result; only the systematic uncertainty is given since it is dominant. This uncertainty was obtained by scaling the one published in [2] for the cross section measured over the range $|t| < 0.5$ GeV^2 by the ratio of the cross sections for the present t range and for $|t| < 0.5$ GeV^2.

The major sources of systematic uncertainty on b and σ are the acceptance determination and the background contamination, the former being dominant. Table 1 lists the individual contributions. In the following we discuss them in detail.

1. In order to estimate the uncertainty due to the acceptance, the analysis was repeated varying the requirements and procedures as listed below.

Contribution	$\lvert\Delta b/b\rvert$	$\lvert\Delta\sigma/\sigma\rvert$
Integrated luminosity	-	1.5%
Acceptance: trigger efficiency	-	9%
Acceptance for pion tracks	$< 1\%$	1%
Acceptance for proton track	7%	6%
Acceptance: sensitivity to binning in t	2%	-
Acceptance: unfolding of beam transverse momentum spread	7%	-
Acceptance: sensitivity of p beam angle	3%	1%
Background: beam-halo	4%	-
Procedure to extract the resonant part of the cross section	1.6%	4%
Background due to elastic ω and ϕ production	-	1%
Radiative corrections	-	4%
Total	11%	12%

Table 1: Contributions to the systematic uncertainty on b and σ.

(a) For the pion tracks in the central detector:

- The pseudorapidity $\eta = -\ln\tan(\theta/2)$ of each of the two tracks was restricted to the range $|\eta| < 1.8$, thereby using only tracks which have traversed at least three superlayers in the CTD.
- The radial distance of the vertex from the beam axis was required to be less than 1 cm.

In both cases the changes are small; by summing them in quadrature one finds $|\Delta b/b| = 0.2\%$ and $|\Delta\sigma/\sigma| = 1\%$.

(b) For the proton track in the LPS:

- The maximum allowed value of χ^2/ndf for the reconstructed proton track was reduced from 6 to 2.
- The minimum distance of approach of the proton trajectory to the beam pipe was increased from 0.5 mm to 1.5 mm.
- Events with $p_X > 0$ and with $p_X < 0$ were analysed separately, as a check of possible relative rotations of the stations.
- The data were divided into a "large acceptance" and a "low acceptance" sample depending on the position of the LPS stations, which, as discussed above, varied slightly from run to run.

By summing the individual contributions to $\Delta b/b$ in quadrature, independently of their sign, $|\Delta b/b| = 7\%$ is obtained. The corresponding uncertainty on σ is $|\Delta\sigma/\sigma| = 6\%$.

(c) The sensitivity of the result on b to the binning in t was studied by reducing bin sizes by up to 20%; the bin edges were moved by up to one fourth of the bin size.

The largest effect was 2% for $|\Delta b/b|$.

(d) As discussed earlier, t has been obtained as $-p_T^2$, with $p_T^2 = p_X^2 + p_Y^2$ the transverse momentum of the scattered proton with respect to the incoming beam axis. Since the incoming proton beam has an intrinsic transverse momentum spread of $\sigma_{p_X} \approx 40$ MeV and $\sigma_{p_Y} \approx 90$ MeV, which is much larger than the LPS resolution in transverse momentum, the measured value of t is smeared with respect to the true t. The Monte Carlo simulation takes into account the proton beam transverse momentum spread. The acceptance corrected t distribution is thus corrected also for this effect.

The following alternative approach to account for the effect of the transverse momentum spread of the beam has also been followed. Assuming that the true t distribution has the form given by equation (9), the measured p_T^2 distribution can be expressed as a convolution of equation (9) and a two-dimensional Gaussian distribution representing the beam transverse momentum distribution, with standard deviations σ_{p_X} and σ_{p_Y}. Unfolding the contribution of the beam transverse momentum spread from $d\sigma/dp_T^2$ provides an alternative evaluation of $d\sigma/dt$. In this case one first measures the distribution of p_T^2 without making any correction for the effects of the beam intrinsic spread, thereby exploiting the good resolution of the LPS on the transverse momentum. In a second stage, the effect of the beam spread is unfolded. If $\sigma_{p_X} = 40$ MeV and $\sigma_{p_Y} = 90$ MeV (as seen in the data, cf. Fig. 5), then $|\Delta b/b| = 7\%$, with only a weak dependence on the values of σ_{p_X} and σ_{p_Y}.

(e) The sensitivity to the determination of the proton beam angle (cf. section 2.2.4) was evaluated by systematically shifting p_T by 10 MeV. This amount is twice the p_T resolution of the LPS and corresponds to > 5 times the uncertainty on the means of the distributions of Fig. 5. The corresponding variations of b and σ were $|\Delta b/b| = 3\%$ and $|\Delta\sigma/\sigma| = 1\%$.

The differences between the values of b obtained in cases (a) to (e) and that obtained with the standard analysis were summed in quadrature, yielding $|\Delta b/b| = 10.5\%$ and $|\Delta\sigma/\sigma| = 6\%$.

2. Effect of background contamination.

(a) As mentioned above, no correction was applied for a possible t dependence of the background. The only significant background is the halo. If the assumption is made that the halo contribution ($5.0\% \pm 0.6\%$) has a distribution of the type $\exp(-b_{halo}|t|)$, then $|\Delta b/b| < 4\%$ when b_{halo} is varied between 5 and 15 GeV^{-2}; this range of variation is consistent with estimates of b_{halo} based on the $ep \to eXp$ events at $Q^2 > 4$ GeV^2 discussed in section 3.3.

(b) If the t dependence of c_{res} evaluated in [2] is assumed for the present data, the slope changes by $\Delta b/b = -1.6\%$.

The latter two contributions were also added quadratically to the systematic uncertainty, yielding a total systematic uncertainty of 11% on b, dominated by the LPS acceptance and the effect of the beam transverse momentum spread.

The total systematic uncertainty on σ is 12%, which includes, in addition to the contributions detailed above, the uncertainty on the luminosity (1.5%), that on the trigger efficiency [2] (9%)

and that related to the extraction of the resonant part of the cross section. The estimated background due to elastic ω and ϕ production, as well as the upper limit of the correction for radiative effects have also been included. The systematic uncertainty on σ is dominated by contributions not related to the LPS (11%); the uncertainty on the LPS acceptance is 6%, which has only a small effect on the total uncertainty when summed in quadrature with the other contributions.

5 Conclusions

The Leading Proton Spectrometer of ZEUS is a large scale system of silicon micro-strip detectors which have been successfully operated close to the HERA proton beam (typically a few mm) by means of the "Roman pot" technique. It measures precisely the momentum of high energy scattered protons, with accuracies of 0.4% for the longitudinal and 5 MeV for the transverse momentum.

As a first application, the cross section, the $M_{\pi\pi}$ and the t dependences of the reaction $\gamma p \to \rho^0 p$ have been measured in the kinematic range $Q^2 < 1$ GeV^2, $50 < W < 100$ GeV, $0.55 < M_{\pi\pi} < 1.2$ GeV and $0.073 < |t| < 0.40$ GeV^2. Elastic events were tagged by demanding that x_L be larger than 0.98, i.e. that the scattered proton carry at least 98% of the incoming proton momentum. For the first time at these energies, t was measured directly. Compared to our previous analysis, the present technique based on the use of the LPS eliminates the contamination from events with diffractive dissociation of the proton into low mass states.

In the range $0.073 < |t| < 0.40$ GeV^2, the differential cross section $d\sigma/dt$ is described by an exponential distribution with a slope parameter $b = 9.8 \pm 0.8$ (stat.) ± 1.1 (syst.) GeV^{-2}. The systematic uncertainty is dominated by the uncertainty on the LPS acceptance and the effect of the intrinsic transverse momentum spread of the beam. In the measured t and $M_{\pi\pi}$ intervals, the integrated ρ^0 photoproduction cross section at $\langle W \rangle = 73$ GeV was found to be 5.8 ± 0.3 (stat.) ± 0.7 (syst.) μb, consistent with our previous measurement [2] obtained in a slightly different kinematic range.

6 Acknowledgements

We thank the DESY directorate for their strong support and encouragement. We are also very grateful to the HERA machine group: collaboration with them was crucial to the successful installation and operation of the LPS.

We also want to express our gratitude to all those who have participated in the construction of the LPS, in particular to the very many people from the University of Bologna and INFN Bologna (B), CERN (C), the University of Calabria and INFN Cosenza (Cs), DESY (D), LAA (L) [31], the University of Torino and INFN Torino (T), the University of California at Santa Cruz (S), who have so greatly contributed to the LPS project at various stages.

For financial support we are grateful to the Italian Istituto Nazionale di Fisica Nucleare (INFN), to the LAA project and to the US Department of Energy.

For the mechanical design and construction of the stations and their interface with HERA: G. Alfarone[T], F. Callà[T], J. Dicke[D], G. Dughera[T], P. Ford[L], H. Giesenberg[D], R. Giesenberg[D], G. Giraudo[T], M. Hourican[L], A. Pieretti[B], P. Pietsch[D].

For discussions on the optical design and on the mechanical interface with HERA and for making some modifications to the machine layout to improve the LPS acceptance: W. Bialowons[D], R. Brinkman[D], D. Degele[D], R. Heller[D], B. Holzer[D], R. Kose[D], M. Leenen[D], G. Nawrath[D], K. Sinram[D], D. Trines[D], T. Weiland[D] and F. Willeke[D].

For advice on radiation doses and hardness of service electronics: H. Dinter[D], B. Lisowski[B] and H. Schoenbacher[C].

For metrology and survey: C. Boudineau[C], R. Kus[D], F. Loeffler[D] and the DESY survey team.

For special monitor information from HERA and the design of the interlock system: P. Duval[D], S. Herb[D], K.-H. Mess[D], F. Peters[D], W. Schuette[D], M. Wendt[D].

For installation and services: W. Beckhusen[D], H. Grabe-Celik[D], G. Kessler[D], G. Meyer[D], N. Meyners[D], W. Radloff[D], U. Riemer[D] and F.R. Ullrich[D].

For developing elliptical cutting of detectors: N. Mezin[C] and I. Sexton[C].

For vacuum design, testing and urgent repairs: R. Hensler[D], J. Kouptsidis[D], J. Roemer[D] and H-P. Wedekind[D].

For front-end electronics design and front-end assembly: D. Dorfan[S], J. De Witt[S], W.A. Rowe[S], E. Spencer[S] and A. Webster[S].

For the development of the special multi-layer boards which support the detectors and the front-end electronics: A. Gandi[C], L. Mastrostefano[C], C. Millerin[C], A. Monfort[C], M. Sanchez[C] and D. Pitzl[S], a former member of ZEUS.

For the loan of S5 and S6 and part of their modification as well as help with urgent repairs: B. Jeanneret[C], R. Jung[C], R. Maleyran[C] and M. Sillanoli[C].

For service, control and readout electronics: F. Benotto[T], M. Ferrari[B], H. Larsen[L], F. Pellegrino[Cs], J. Schipper[L], P.P. Trapani[T] and A. Zampieri[T].

References

[1] ZEUS Collab., M. Derrick et al., Phys. Lett. **B 315** (1993) 481;
H1 Collab., T. Ahmed et al., Nucl. Phys. **B429** (1994) 477;
ZEUS Collab., M. Derrick et al., Phys. Lett. **B 332** (1994) 228;
H1 Collab., T. Ahmed et al., Phys. Lett. **B 348** (1995) 681;
ZEUS Collab., M. Derrick et al., Z. Phys. **C 68** (1995) 569;
ZEUS Collab., M. Derrick et al., Phys. Lett. **B 346** (1995) 399;
ZEUS Collab., M. Derrick et al., Phys. Lett. **B 356** (1995) 129;
ZEUS Collab., M. Derrick et al., Z. Phys. **C 70** (1996) 391.

[2] ZEUS Collab., M. Derrick et al., Z. Phys. **C 69** (1995) 39.

[3] H1 Collab., S. Aid et al., Nucl. Phys. **B463** (1996) 3.

[4] H1 Collab., T. Ahmed et al., Phys. Lett. **B 338** (1994) 507;
H1 Collab., S. Aid et al., DESY report DESY 96-037 (1996).

[5] ZEUS Collab., M. Derrick et al., Phys. Lett. **B 350** (1995) 120.

[6] ZEUS Collab., M. Derrick et al., Phys. Lett. **B 356** (1995) 601.

[7] H1 Collab., S. Aid et al., Nucl. Phys. **B468** (1996) 3.

[8] U. Amaldi et al., Phys. Lett. **43B** (1973) 231.

[9] For a review, see e.g. T.H. Bauer et al., Rev. Mod. Phys. **50** (1978) 261.

[10] R. M. Egloff et al., Phys. Rev. Lett. **43** (1979) 657.

[11] OMEGA Photon Collab., D. Aston et al., Nucl. Phys. **B209** (1982) 56.

[12] ZEUS Collab., M. Derrick et al., The ZEUS Detector, Status Report 1993, DESY (1993).

[13] ZEUS Collab., M. Derrick et al., Phys. Lett. **B 293** (1992) 465.

[14] C. Alvisi et al., Nucl. Instr. and Meth. **A305** (1991) 30.

[15] N. Harnew et al., Nucl. Instr. Meth. **A279** (1989) 290;
B.Foster et al., Nucl. Phys., Proc. Suppl. **B32** (1993) 181;
B.Foster et al., Nucl. Instr. Meth. **A338** (1994) 254.

[16] M.Derrick et al., Nucl. Instr. Meth. **A309** (1991) 77;
A.Andresen et al., Nucl. Instr. Meth. **A309** (1991) 101;
A.Bernstein et al., Nucl. Instr. Meth. **A336** (1993) 23;
A.Caldwell et al., Nucl. Instr. Meth. **A321** (1992) 356.

[17] J. Andruszków et al., DESY report DESY 92-066 (1992);
ZEUS Collab., M.Derrick et al., Z. Phys. **C 63** (1994) 391.

[18] R. Battiston et al., Nucl. Instr. and Meth. **A238** (1985) 35.

[19] D.E. Dorfan, Nucl. Instr. and Meth. **A342** (1994) 143;
E. Barberis et al., Nucl. Phys. **B32** (Proc. Suppl.) (1993) 513.

[20] J. DeWitt, Nucl. Instr. and Meth. **A288** (1990) 209;
J. DeWitt, "The Time Slice Chip", Senior Thesis (1989), UC Santa Cruz, Santa Cruz Institute for Particle Physics report SCIPP 89-24.

[21] ZEUS Collab., "A Forward Neutron Calorimeter for ZEUS", DESY PRC 93-08;
S. Bhadra et al., Nucl. Instr. and Meth. **A354** (1995) 479.

[22] R. Sacchi, "Studio di eventi diffrattivi con uno spettrometro per protoni a ZEUS", Tesi di Dottorato, University of Torino (1996), unpublished (in Italian).

[23] M. Arneodo, L. Lamberti and M. G. Ryskin, DESY Report DESY 96-149 (1996), to appear in Comp. Phys. Comm.

[24] K. Schilling et al., Nucl. Phys. **B15** (1970) 397;
K. Schilling and G. Wolf, Nucl. Phys. **B61** (1973) 381.

[25] T. Sjöstrand, Comp. Phys. Comm. **82** (1994) 74.

[26] T.J. Chapin et al., Phys. Rev. **D31** (1985) 17.

[27] CDF Collab., F. Abe et al., Phys. Rev. **D50** (1994) 5535.

[28] K. Kurek, private communication.

[29] S.D. Drell, Phys. Rev. Lett. **5** (1960) 278.

[30] P. Söding, Phys. Lett. **19** (1966) 702.

[31] G. Anzivino et al., Rivista del Nuovo Cimento, Vol. 13, no. 5 (1990) 1.

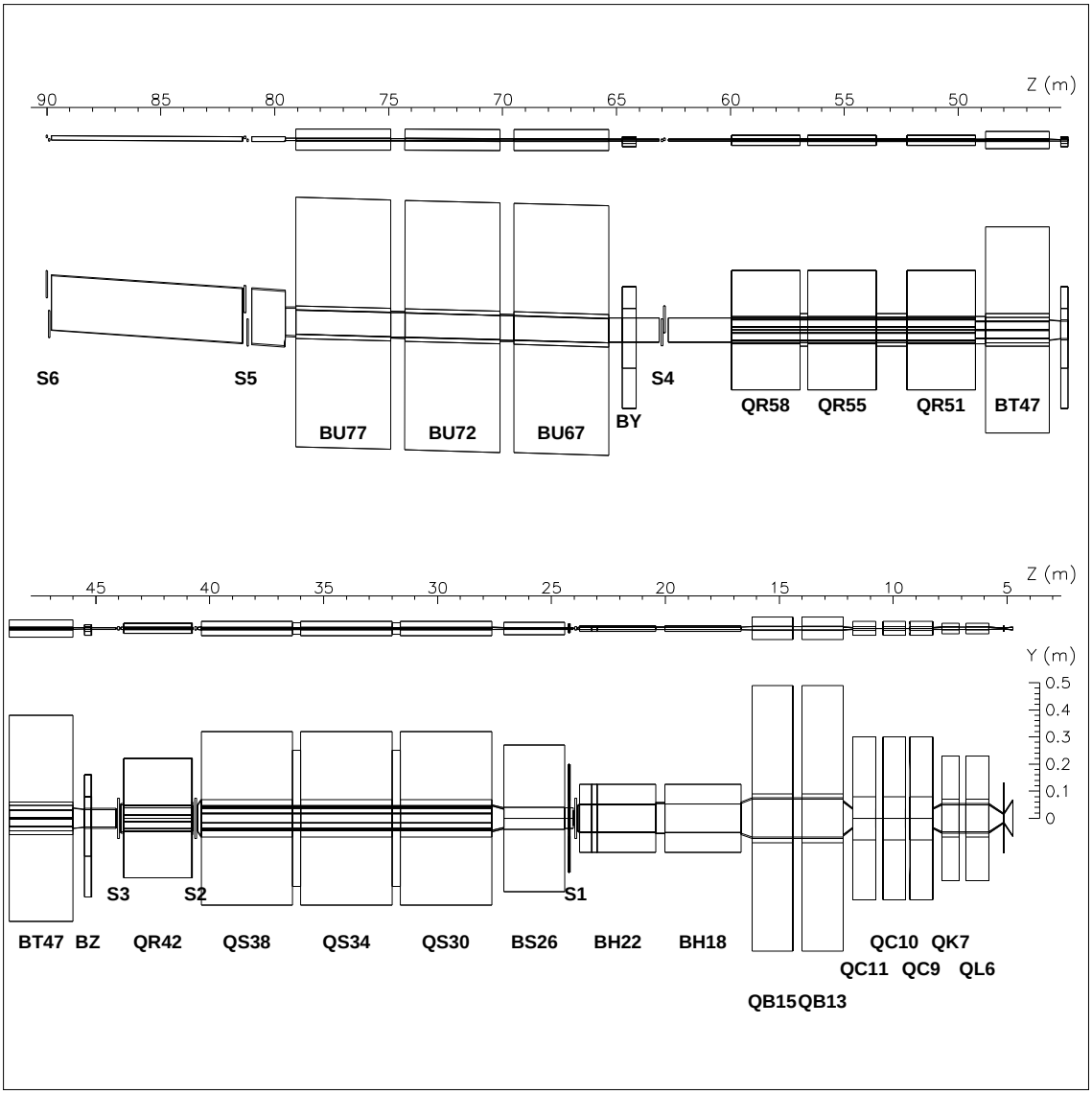

Figure 1: Side view of the outgoing proton beam line for Z between 5 and 50 m (bottom) and between 50 and 90 m (top). The small drawing below the Z axis is to scale; in the large drawing different scales are used for the longitudinal and transverse directions. Magnetic elements labelled BH, BS and BT are horizontally bending dipoles; vertically bending dipoles are indicated as BZ, BY and BU. Quadrupoles are labelled as QL, QK, QC, QB, QS, QR; the magnets upstream of the septum magnet BS are common to the proton and positron beam line. The positions of the LPS stations S1 through S6 are also shown. The centre of the ZEUS detector is at $Z = 0$.

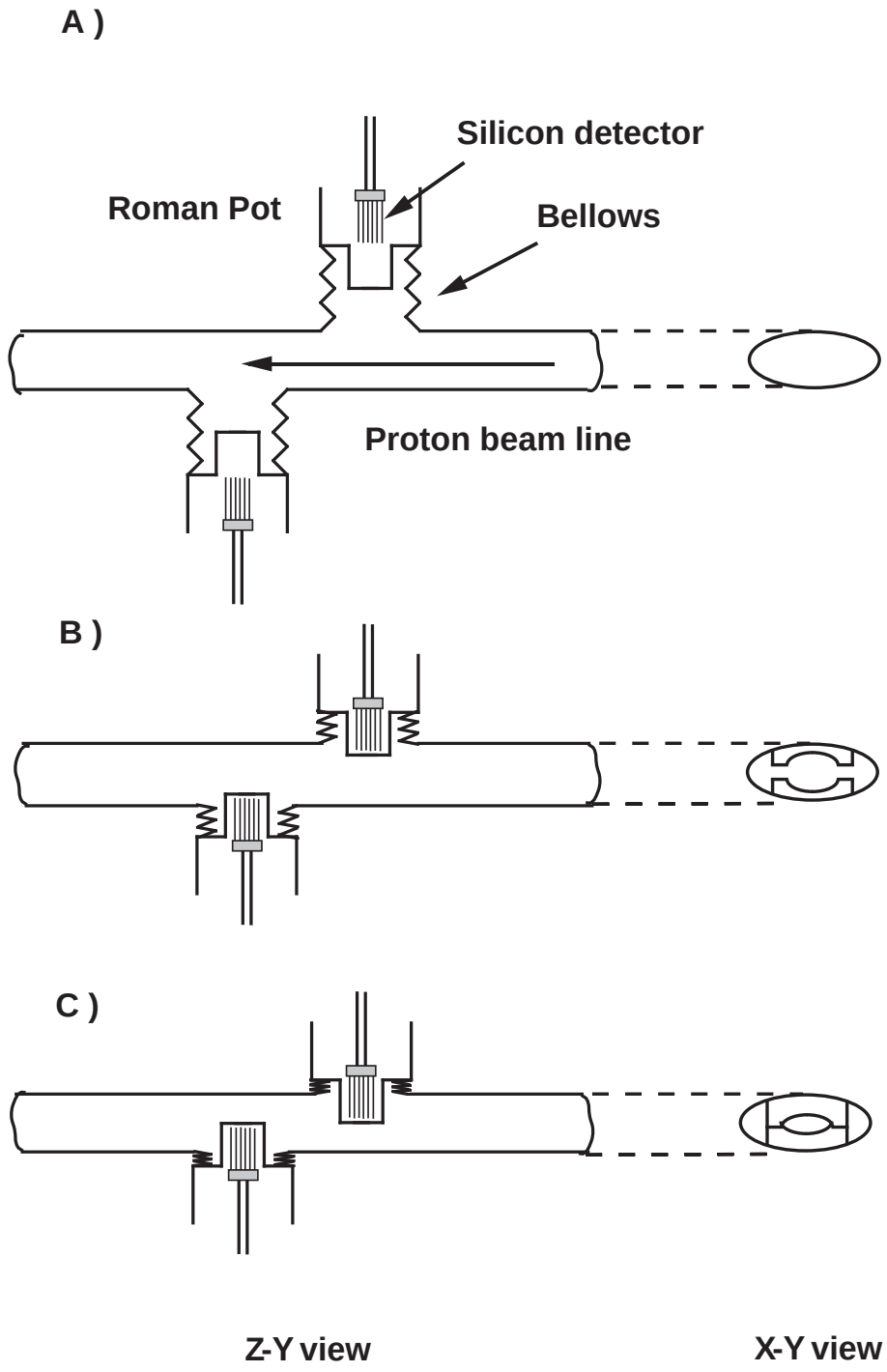

Figure 2: Schematic layout of a station (like S4, S5 or S6). A) During beam filling and ramping, the detector planes (labelled "Silicon detector") are kept outside of the pots and the pots are placed far from the beam. The zig-zag lines indicate the bellows. B) The detector planes are inside the pots and the pots are being moved towards the beam. Note the elliptical profile of the fronts of the pots (X-Y view), which matches the cutout of the detector planes. C) When taking data, the pots are fully inserted and the detector planes in the upper and lower half of the station partially overlap in the transverse plane.

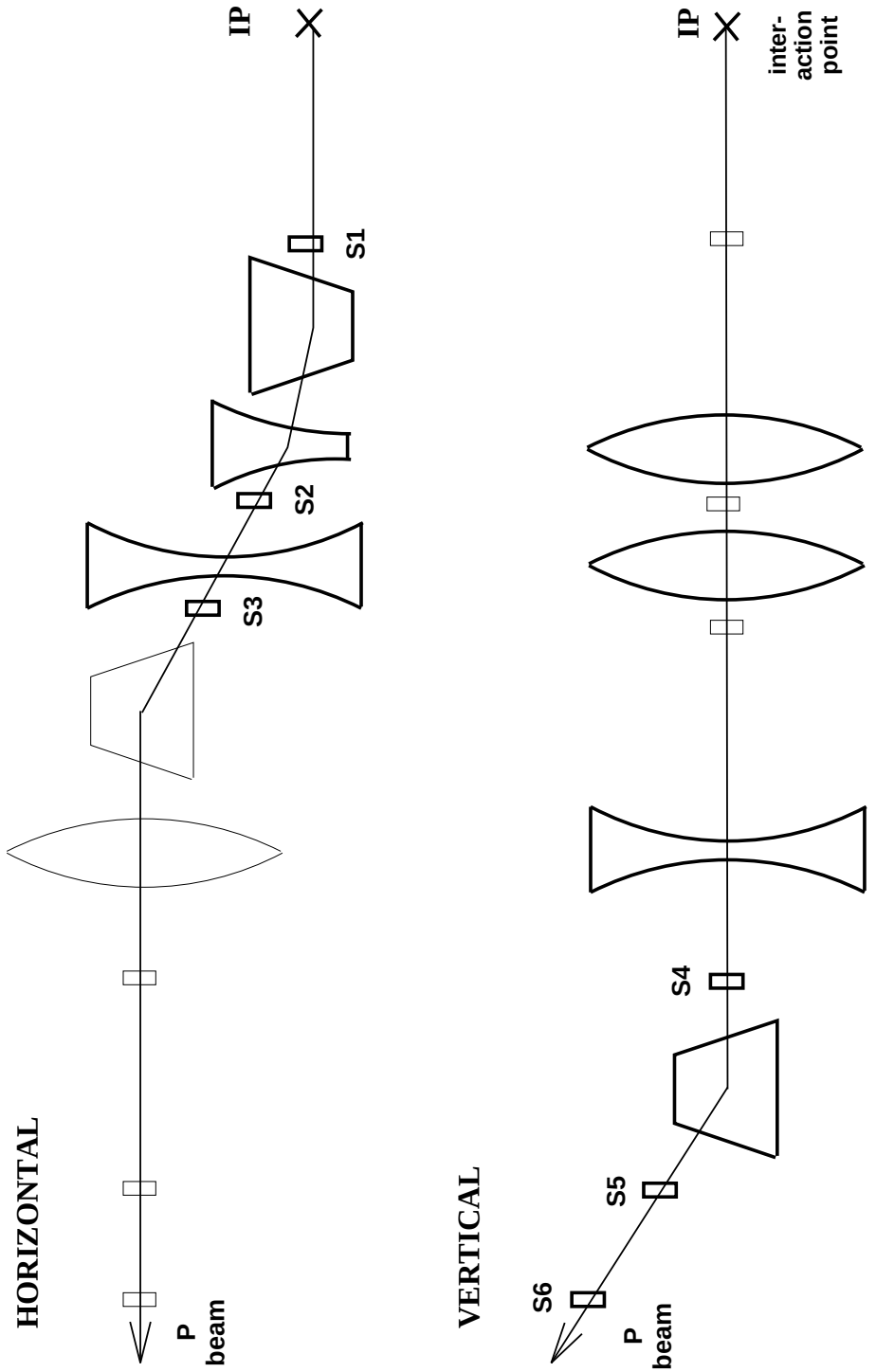

Figure 3: Simplified diagram of the HERA proton beam optics relevant for the LPS. The top view (labelled "horizontal") shows the magnetic elements relevant to the S1, S2 and S3 spectrometer as thick lines. Note the half quadrupole between S1 and S2. The side view (labelled "vertical") shows the magnetic elements relevant to the S4, S5 and S6 spectrometer as thick lines.

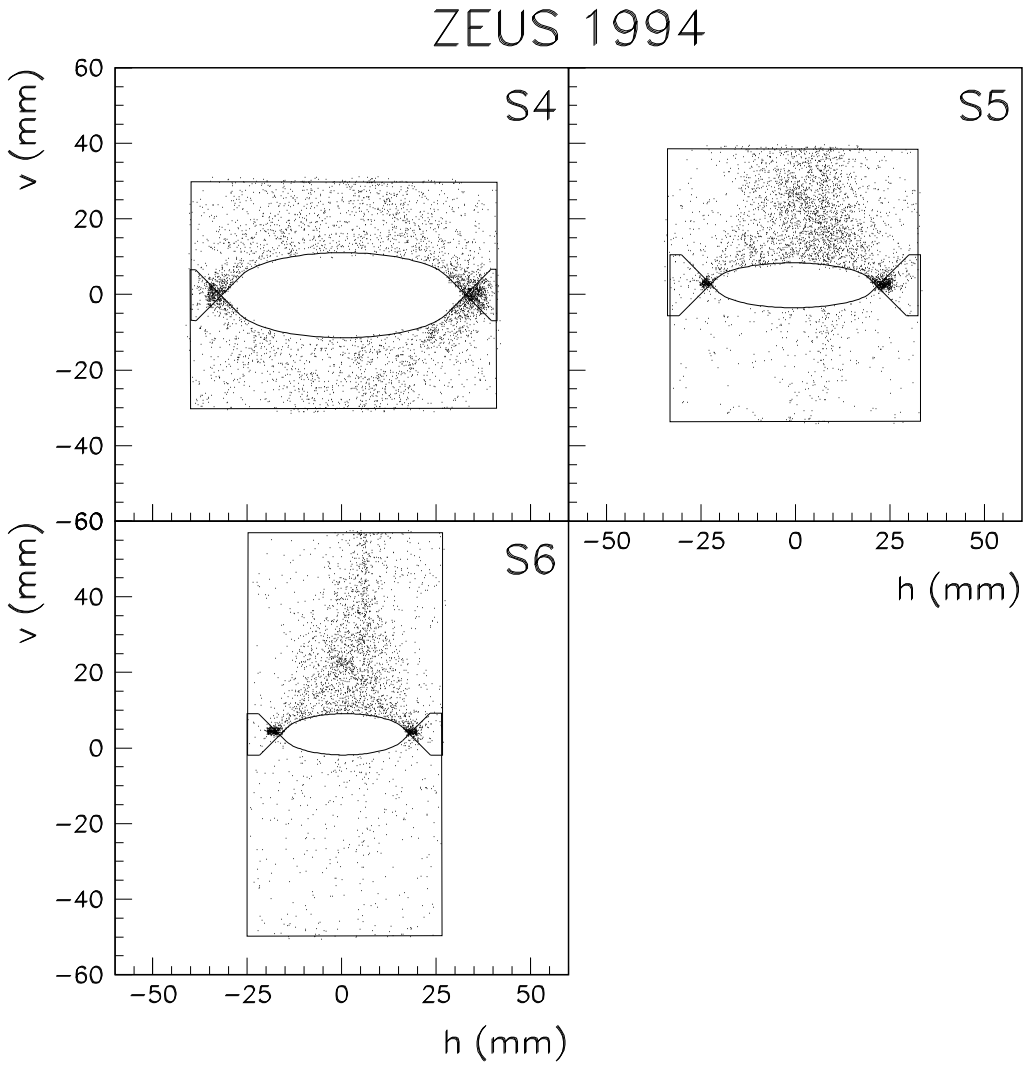

Figure 4: Positions of the reconstructed track impact points in S4, S5 and S6. For each plot the origin of the reference frame coincides with the position of the nominal proton beam at the value of Z corresponding to the centre of the station. The continuous lines approximately indicate the sensitive region of the detector planes.

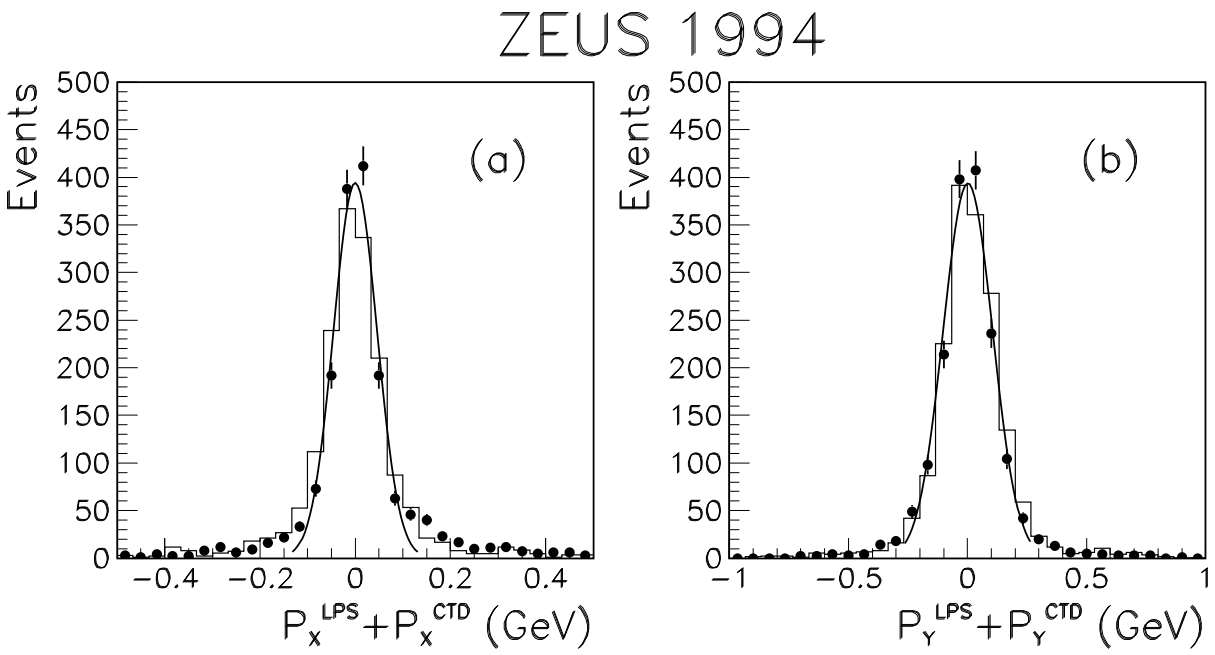

Figure 5: Sum of the X (a) and Y (b) components of the proton momentum as measured by the LPS and of the ρ^0 momentum as measured by the CTD. The histogram was obtained with the Monte Carlo simulation discussed in section 3.2. The continuous line is the result of a Gaussian fit to the data. The fitted values of the standard deviations are 45 and 102 MeV, respectively. They are dominated by the spread of the transverse momentum in the beam. The other minor contributions are the LPS and CTD resolutions and the fact that Q^2 is not exactly zero; events with $Q^2 \gtrsim 0.01$ GeV^2 contribute to the non-Gaussian tails.

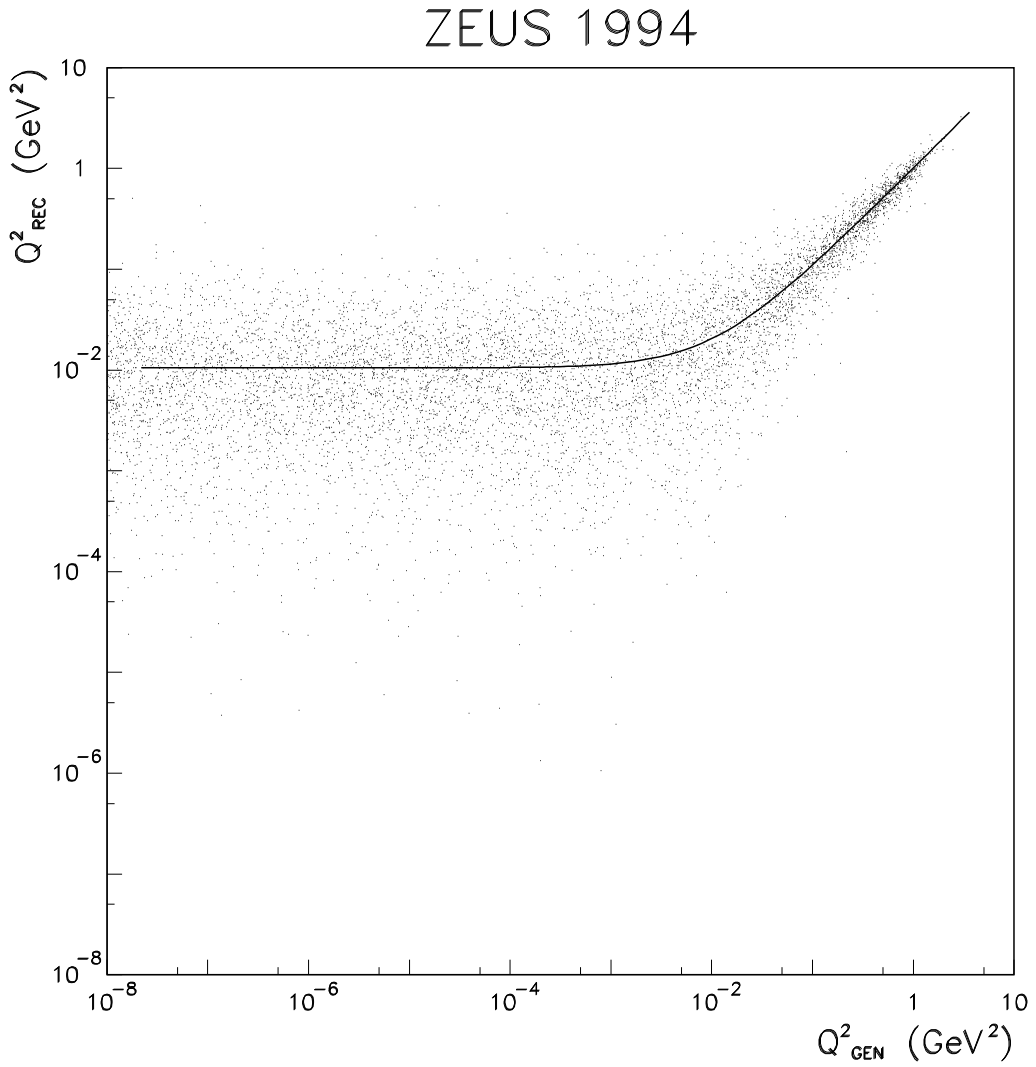

Figure 6: Scatter plot of reconstructed versus generated values of Q^2 for Monte Carlo events. The continuous line shows the expected average relation assuming a spread of the beam transverse momentum with standard deviations $\sigma_{p_X} = 40$ MeV and $\sigma_{p_Y} = 90$ MeV in the horizontal and in the vertical directions, respectively.

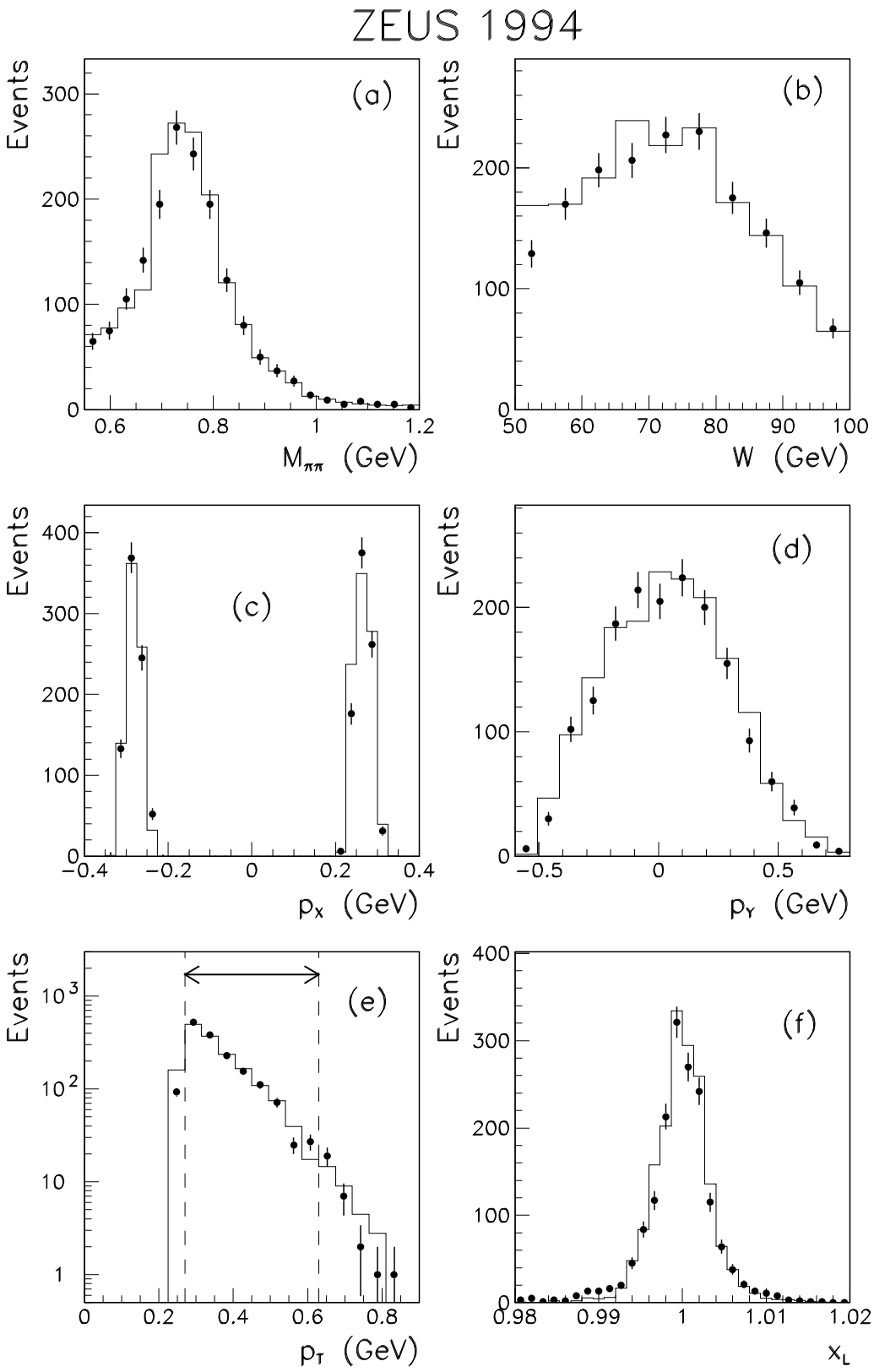

Figure 7: Observed distributions for (a) $M_{\pi\pi}$, (b) W, (c) p_X, (d) p_Y, (e) p_T and (f) x_L of the reconstructed data (points) and the reconstructed Monte Carlo events (histogram). The distributions are not corrected for acceptance. The vertical bars indicate the statistical uncertainties. The dashed lines in (e) show the limits of the p_T region used.

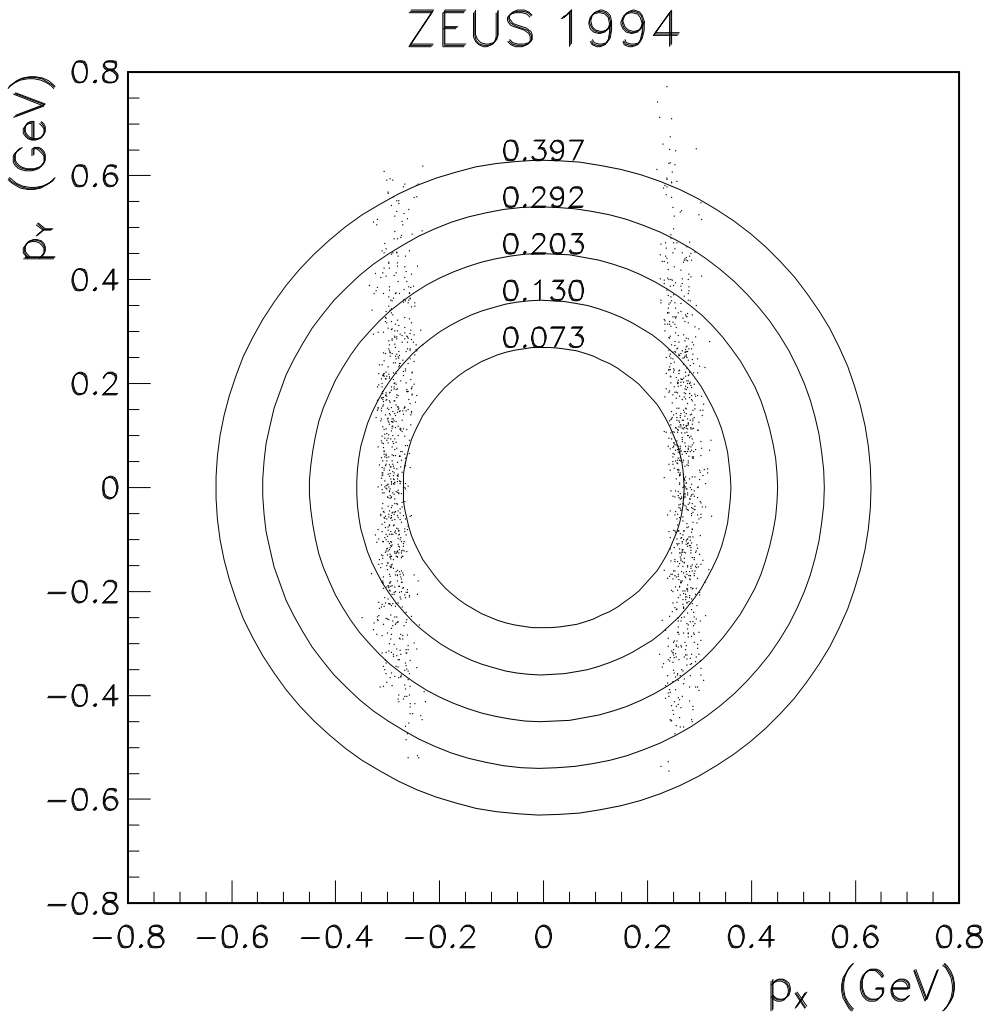

Figure 8: Scatter plot of the X and Y components of the scattered proton momentum as measured by the LPS for the accepted events. The continuous curves correspond to the indicated values of $|t|$ (in GeV^2), which were used as limits of the bins in Fig. 13.

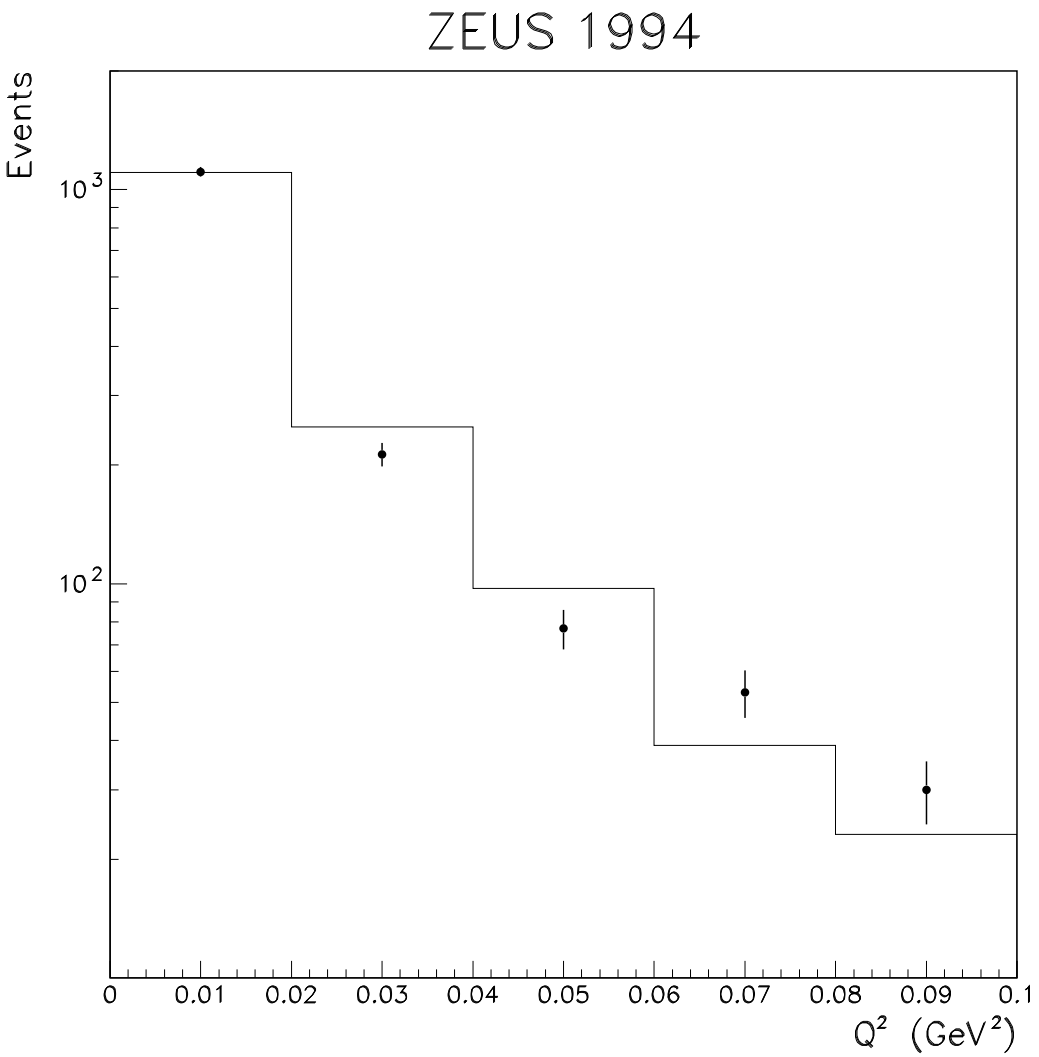

Figure 9: Q^2 distributions of the reconstructed data (points) and the reconstructed Monte Carlo events (histogram). The distributions are not corrected for acceptance. Only the region $Q^2 < 0.1$ is shown. The vertical bars indicate the size of the statistical uncertainties.

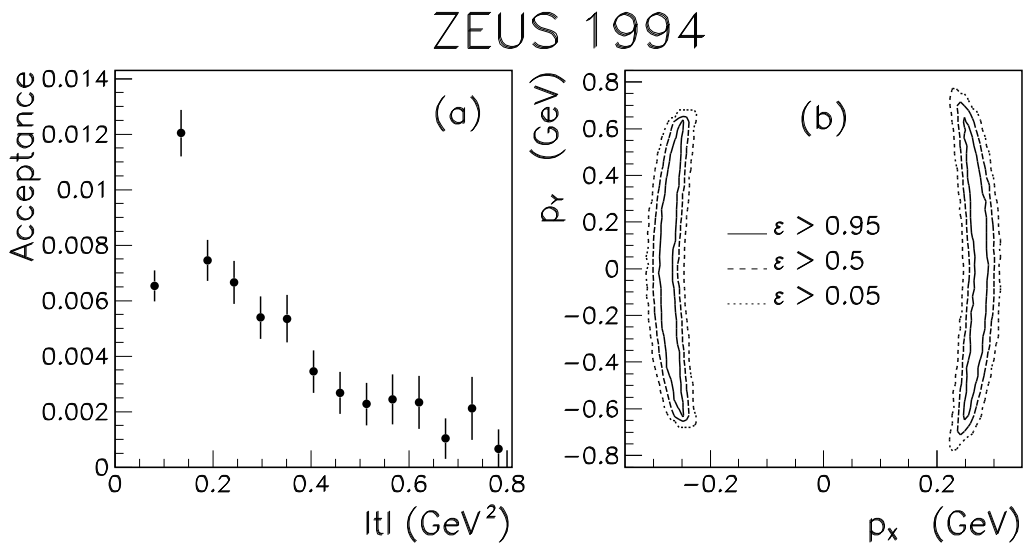

Figure 10: (a) Acceptance as a function of t; it includes the effects of the geometric acceptance of the apparatus (ZEUS and LPS), of its efficiency and resolution and of the trigger and reconstruction efficiencies. The vertical bars indicate the size of the statistical uncertainties. (b) Purely geometric acceptance ε for the LPS alone for $x_L = 1$ tracks as a function of p_X and p_Y.

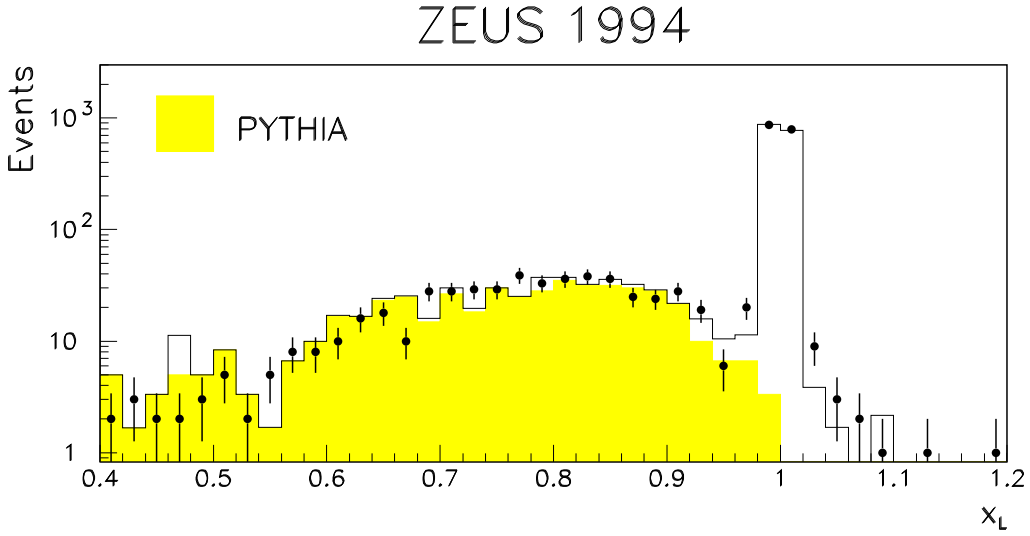

Figure 11: Reconstructed x_L spectrum for the data (points). All selection cuts were applied except that on x_L. The distribution is not corrected for acceptance. The sum of the reconstructed x_L distributions produced with the DIPSI and PYTHIA generators was fitted to this spectrum with the normalisations as free parameters of the fit. The result of the fit is shown as a histogram. The DIPSI generator simulates the elastic reaction $ep \to e\rho^0 p$, and PYTHIA the proton dissociative reaction $ep \to e\rho^0 X_N$. The contribution of PYTHIA is shown as the hatched area. The vertical bars indicate the size of the statistical uncertainties.

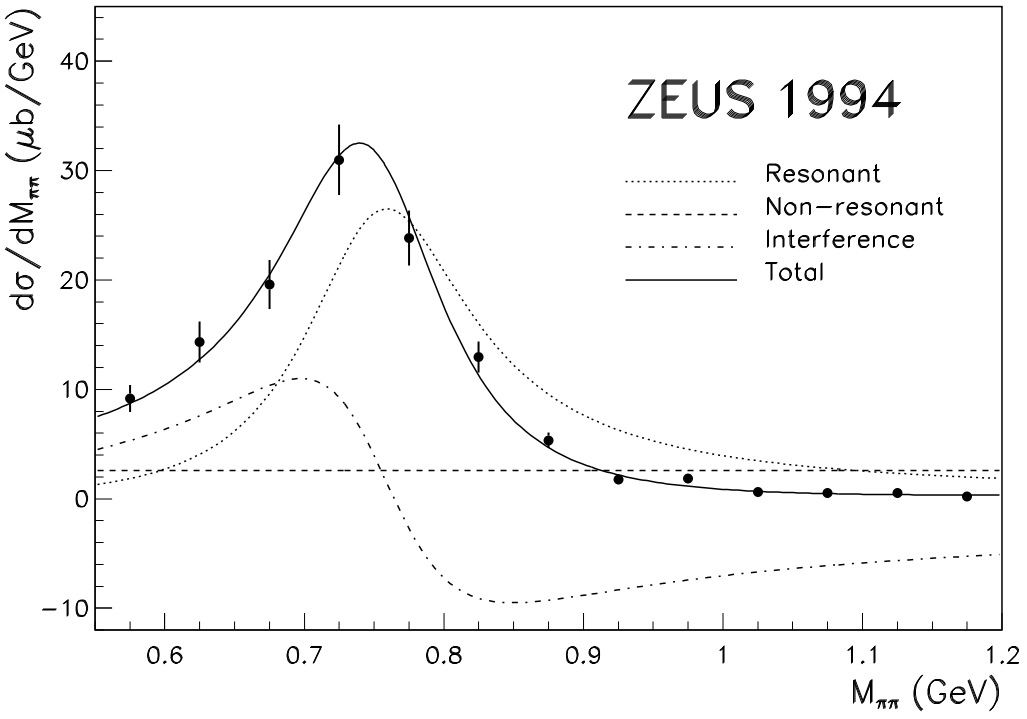

Figure 12: Differential cross section $d\sigma/dM_{\pi\pi}$ for the reaction $\gamma p \to \pi^+\pi^- p$, in the region $0.55 < M_{\pi\pi} < 1.2$ GeV and for $\langle W \rangle = 73$ GeV. The vertical bars indicate the size of the statistical uncertainties only. The lines indicate the result of the fit using expression (11) of ref. [2].

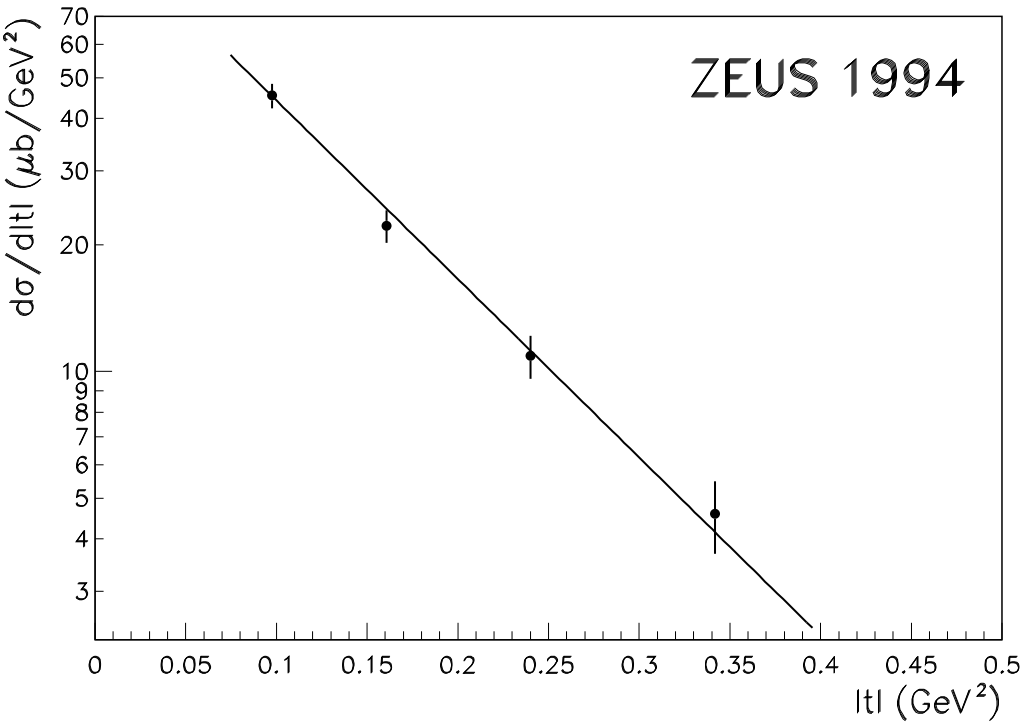

Figure 13: Differential cross section $d\sigma/d|t|$ for elastic ρ^0 photoproduction, $\gamma p \to \rho^0 p$, at $\langle W \rangle = 73$ GeV in the region $0.073 < |t| < 0.40$ GeV^2, $0.55 < M_{\pi\pi} < 1.2$ GeV. The vertical bars indicate the size of the statistical uncertainties only. The line is the result of the fit described in the text.